AIAA '89

AIAA-89-1105

Review of Sonic Boom Theory

K. J. Plotkin, Wyle Laboratories
Arlington, VA

AIAA 12th Aeroacoustics Conference
April 10-12, 1989 / San Antonio, TX

REVIEW OF SONIC BOOM THEORY

Kenneth J. Plotkin
Principal Scientist
Wyle Laboratories
Arlington, Virginia

Abstract

A review is presented of sonic boom theory, covering three viewpoints: historical perspective, an exposition of established boom theory and special phenomena, and the theoretical needs of current sonic boom problems. The review is intended to serve as a tutorial for the non-specialist as well as a review of the current state-of-the-art and open issues. The greatest interest in sonic boom was associated with SST projects of the 1960s, and much of sonic boom theory has been shaped by that influence. Major elements of sonic boom analysis have been well established into what may be called standard theory. Current sonic boom problems require elements beyond standard theory, including the influence of hypersonic speeds, better integration of sonic boom analysis into the aircraft design process, and a more complete understanding of focal zones.

1. Introduction

Historical Background

Prior to the first supersonic flight by aircraft, sonic booms had not been explicitly anticipated. They were at first regarded as a unique or curious phenomenon. Early theories of the cause of sonic boom speculated on the coalescence of sound as an aircraft broke the sound barrier.[1,2] Research through the early to mid-1950s showed, however, that sonic boom is simply the shock wave pattern associated with supersonic flight. A key factor in this finding was the existence of far-field shock wave analysis from the ballistic projectile community in the 1940s and earlier. An analysis by Landau[3] of weak shock waves predicted the now-familiar N-wave far-field signature. Measurements, in the 1940s, of projectile shock waves clearly exhibited this structure and established scaling laws for the amplitude and duration of far-field N-waves.[4] Whitham's classic paper in 1952 provided an elegant and consistent theoretical description of the phenomenon.[5] While this paper talked of "projectile" and "flow pattern", not "aircraft" or "boom", a simple change of nomenclature made it the cornerstone of sonic boom theory. Through the 1950s and 1960s, sonic boom theory evolved into a fairly complete understanding for nominal flight of supersonic aircraft (including the effect of lift) in a real atmosphere (including the effect of wind, density, and temperature gradients).

The 1960s saw intense sonic boom research activity associated with the Anglo-French Concorde, the American SST, and the Soviet Tu-144. This research led to the completion of what may be called "standard" sonic boom theory, plus varying degrees of progress in special sonic boom phenomena such as the effects of hypersonic speeds and the nature of focused "superbooms". Psycho- and socioacoustic research showed, however, that sonic booms of the magnitude generated by the first generation SSTs would not be acceptable in populated areas. This finding was a key factor in the cancellation of the American SST and restriction of Concorde to primarily over-water operations.

With that, sonic boom research dropped to a low level of activity. NASA maintained continuing studies to assess the feasibility of an advanced SST as aircraft technology advanced. A certain degree of sonic boom work was performed in support of environmental assessment and mission planning for the space shuttle, which would have supersonic flight phases over populated areas. Some sonic boom work continued at several universities and research centers, primarily as a scientific endeavor and also to investigate curious boom occurrences from Concorde and supersonic military aircraft.

In the early to mid-1980s, there was a revived interest in supersonic flight which rekindled sonic boom research. This came from three areas. First, NASA's ongoing SST research showed that an advanced long-range SST – the "Orient Express" – may be feasible in the near future. This topic is very closely related to the atmospheric flight phases of the single-stage-to-orbit National Aerospace Plane. Second, sonic boom became an important factor in the environmental planning aspects of military supersonic airspaces. It was found that prediction models from the 1960s and 1970s, with primary emphasis on high-altitude cruise, were not appropriate for analysis of boom from high-speed air combat ("dogfighting") training operations. Third, sonic boom experience had been acquired from space shuttle, and this needed to be reconciled with expectations. It is interesting to note that these three areas, which arose independently of each other, each involve topics which were not fully established as part of the standard boom theory completed by the late 1960s.

Through the mid-1980s to the present, there has been steadily increasing research associated with sonic boom. The purpose of this paper is to present a tutorial and review of the theory. Standard boom theory is presented in some detail. The detail is not sufficient to perform calculations or develop a computer code from this paper alone, but is sufficient to define the theory, its assumptions, and its limitations. Phenomena not within standard theory are hypersonic flight speeds, focused superbooms, shock wave rise times, and atmospheric turbulence effects. Theory for these phenomena is reviewed in sufficient detail so as to describe the current state of understanding.

Earlier Sonic Boom Reviews

There have been a number of previous reviews of sonic boom. Because of the hiatus in sonic boom research, the literature can be divided into what was known as of about 1970 and what has been added since then. Reviews written around that time are of particular interest. There are three in particular which were prepared by key investigators in sonic boom research of that era, and are highly recommended:

- Reference 6 is the documentation of the first fully successful and complete sonic boom computer program. It contains a complete exposition of standard theory and the particular equations and algorithms employed.
- Reference 7 is a review of sonic boom theory. The current paper has drawn on some of the material in that review, and the original is worth examining.
- Reference 8 is a literature review with an excellent summary of the state-of-the-art at that time, and capsule reviews of virtually all the key publications. The review covers sonic boom effects as well as the prediction theory which is the topic of the current review and References 6 and 7.

Several other reviews may be found among the references cited in this paper, but these three are particularly relevant to the current topic.

Organization of Review

There are three basic structures which this review must address. First, sonic boom theory itself is somewhat modular, and application of the basic theory is greatly simplified by recognizing this. Second, it is important to identify the limitations of standard boom theory and approaches to extending it. Third, it is useful to place boom phenomena and the status of various theory elements in the context of the three current areas of interest. To address these needs, this paper is organized in the following way:

- Section 2 is an overview of sonic boom. The physical phenomena involved are described, and the overall structure of boom theory (and its modularity) is presented.

- Section 3 contains a discussion of each of the topics introduced in Section 2. This section contains the details of the theory and governing equations. The discussion in each subsection carries through from standard theory to recent extensions and/or needed future advances.

- Section 4 contains a discussion of how each of the sonic boom elements relates to the needs of each of the three current application areas. Just as sonic boom theory of the 1960s was influenced by the needs of first-generation SSTs, currently developing boom theory will be shaped by the problems at hand.

2. Overview of Sonic Boom Phenomena

Elements of Standard Theory

Figure 1 is a capsule overview of sonic boom generated by a supersonic aircraft flying in a real atmosphere. The figure shows, in aircraft-fixed coordinates, the wave pattern about an aircraft flying from right to left. Several wavefronts are sketched in, as are pressure signatures which might be measured at three distances. The waves shown are in a section under the aircraft; the full three-dimensional wave pattern would be a conical generalization of this figure.

Near the aircraft, there is a pressure field which is directly related to the aerodynamics of the vehicle, and whose structure reflects particular geometric details of the vehicle. In the 1950s, supersonic aircraft aerodynamics was computed by linearized supersonic flow theory[9] and the supersonic area rule.[10,11] This approximation is equivalent to linear acoustics and gives the wave field as well as aerodynamic loads. The wave field is an acoustic field in which all waves are straight line characteristics inclined at the Mach angle. The amplitude on a given characteristic is defined by the aircraft geometry and the axial location of the characteristic, and decreases with the square root of distance from the aircraft. For an axisymmetric projectile, the wave field is axisymmetric. For non-axisymmetric bodies (which is always the case for aircraft with lift), the near field has three-dimensional cross-flow effects, but far from the vehicle the wave field can be treated as locally axisymmetric.

While linearized flow theory predicts straight characteristics, Figure 1 shows curved wavefronts. There are two reasons for this. First, supersonic flow is inherently nonlinear, while linearized theory is an approximation assuming weak waves which propagate at acoustic velocity. The actual flow field has a range of amplitude-dependent wave velocities, and this causes the waves in Figure 1 to have different shapes relative to each other. Second, the atmosphere is not uniform, and sound speed generally decreases with increasing altitude. The resultant refraction causes the overall concave shape of the waves.

The exact flow field about a supersonic body as shown in Figure 1 would have a finite strength shock at the nose, followed initially by expansion waves. These waves would be inclined forward of the Mach waves, with the shock wave inclined less so than the expansion waves. Expansion waves would eventually intersect and merge with the shock, weakening it and causing its angle to approach the Mach angle. For a slender body, this effect is small and the near-field signature is well approximated by the linear theory with Mach-wave characteristics. At large distances, however, the weak nonlinearity does have a significant cumulative effect, causing the signature to distort as sketched for mid- and far-field. Landau[3] showed that the far-field effect of this distortion would be for the forward, positive-pressure, portion of the signature to coalesce into a single shock followed by a linear expansion. The rear part coalesces into a similar expansion followed by a recompression shock, leading to a symmetric N-wave. Whitham[5,12] showed that this process could be modeled as a second-order

approximation built up from the linear acoustic solution. He asserted that the linear amplitude on each characteristic was correct to first order, but that the far-field error was due to the acoustic characteristics (representing propagation at the unperturbed ambient sound speed) being a zero'th order approximation. A uniform first-order solution would have characteristic location corrected by propagation at the first-order perturbed sound speed plus acoustic perturbation velocity. This procedure, known as Whitham's rule, predicts the far-field N-wave and has been well validated as the appropriate approximation for computing the far-field wave shapes of sonic booms. Note that the sketch in Figure 1 shows particular details of the near-field signature associated with particular wavefronts, and these vanish from the near- and far-field signatures as they coalesce with each other and/or are absorbed into shock waves.

The mathematical details of Whitham's rule are presented in the next section. It is worth noting at this time that it amounts to a correction in signature shape which is linear in nature: relative to acoustic propagation speed, each element of the signature advances proportional to its original amplitude. One can compute an "advance" (or "age") parameter which is the advance of a unit-strength wave as a function of distance from the aircraft, and apply this proportionately to each part of the signature. It is also worth noting that high-amplitude parts of the signature will eventually overtake lower amplitude portions ahead, including the unperturbed air ahead of the bow shock. This results in the formation of shock waves, which within the context of this theory are treated as zero-thickness discontinuities. The far-field signature will also be longer than the aircraft or the near-field signature.

The overall curvature of waves due to the sound speed gradient is a refraction effect on the linear acoustic solution, and can be analyzed as a linear acoustic propagation problem. The wave shape sketched in Figure 1 can be computed via wave refraction in aircraft-fixed coordinates, and the corresponding amplitude effects computed from a gasdynamics viewpoint. This procedure can, however, be very difficult to formulate for all but the simplest case of under the flight track when in steady level flight. The general method for tracing sound through a non-uniform medium is to change the reference to medium-fixed coordinates and use the method of geometrical acoustics, or ray-tracing. Figure 2 is a sketch equivalent to Figure 1, but in atmosphere-fixed coordinates. The aircraft is flying from left to right, and boom propagation and evolution is shown along rays. Rays are orthogonal to wavefronts and represent the paths along which the acoustic disturbance propagates. Note that wavefronts shown in Figure 1 exist at a given time, but each point on each wave was generated by the aircraft at some earlier time. The rays shown in Figure 2 are generated at the time the aircraft is at the position shown and represent the trajectories the disturbance will follow as it propagates to the ground. As with Figure 1, this is a section under the aircraft, and there is a corresponding ray-cone pattern in three dimensions.

Geometrical acoustics ray tracing has rules similar to those of geometrical optics. The initial direction of a ray is given by the ray cone near the aircraft, orthogonal to the Mach cone. The atmosphere can very reasonably be modeled as horizontally stratified, so ray shapes are readily traced via Snell's law. Since rays are trajectories along which acoustic energy propagates, a useful concept is the ray tube, a bundle of rays analogous to a stream tube. Energy is conserved along a ray tube, and the amplitude of a pressure wave is related to the energy by the local acoustic impedance and ray tube cross-sectional area. The geometrical acoustics calculation required for sonic boom analysis consists of tracing the ray shapes (and location of ground impingement) and the ray tube area, generally as a differential quantity along each ray path.

The initial rays required for the geometrical acoustics ray tracing calculation depend only on the aircraft location and trajectory, not on the near-field signature. The effect of aircraft maneuvers is automatically handled by this method: a ray tube will include rays

generated at several different times, so that changes in aircraft position, heading, attitude, or Mach number will manifest themselves in the ray tube initial conditions.

Modular Structure of Sonic Boom Theory

The above discussion presents standard sonic boom theory as a set of three elements. This represents a modularity which is quite real, and establishes the structure of virtually all boom calculation schemes. The three elements, and the order in which they are applied, are as follows:

1. The acoustic source signature of the vehicle is obtained, traditionally from linearized flow area rule theory. This is usually presented in a normalized form known as the Whitham F-function. It represents the axisymmetric (or locally axisymmetric) linear acoustic solution in a uniform medium.

2. Geometrical acoustics ray tracing is performed, requiring as inputs the vehicle trajectory and the structure of the atmosphere. The result of this calculation is the locations of the rays and the ray tube areas. Also known from this element is the local acoustic impedance along each ray. This leads to an amplitude expression which may be viewed as a generalization of the square-root-of-distance term in the uniform atmosphere acoustic solution.

3. Whitham's rule is applied to the complete linear acoustic signature (F-function extrapolated to large distances by ray tracing). This accounts for nonlinear steepening or "aging" of the signature. The calculation itself requires, first, calculation of the advance of a unit amplitude wave for the ray solution, and, second, application of this to the original F-function shape.

These three steps are illustrated in Figure 3. Part (a) is the acoustic source, (b) shows the effect of acoustic propagation where amplitude changes but the shape is fixed, and (c) shows non-linear steepening proportional to an age parameter and the amplitude of each element of the original F-function. Part (c) also shows positions where the steepening construction results in triple-valued regions. These are locations where shock waves have formed, and the shocks are inserted by an "area-balancing" rule which will be discussed later.

Limitations of Standard Boom Theory

In the introduction, it was noted that there are several phenomena of interest that are beyond the capability of the standard theory. These are:

Hypersonic flight. The aircraft source F-function is typically obtained from linearized flow area rule theory. This is valid for slender bodies at moderate supersonic Mach numbers. For high-speed or blunt vehicles, the vehicle flow field must be analyzed by other means. At some radius which is large compared to vehicle dimensions, there will be a locally axisymmetric acoustic pressure field. This distance must be identified, an effective F-function written, and the ray tracing begun from there.

Focused "superbooms". Considering the analogy between geometrical acoustics and geometrical optics, one might expect focal zones where ray tube area vanishes and the acoustic solution is singular. Such regions can occur for credible aircraft flight conditions and/or maneuvers.

Shock wave rise times. Standard theory represents shock waves in the traditional gas-dynamic form of zero-thickness pressure jumps. Real sonic boom shock waves have

a finite rise time which affects the high-frequency content of the boom spectrum. The frequencies affected are important for some human-response loudness assessment techniques. In those cases, some type of shock structure model is required.

Atmospheric turbulence effects. Flight test measurements of sonic booms generally agree very well with predictions. Under unstable turbulent atmospheric conditions, however, there are random variations in amplitude, random fine-structure perturbations superposed on the basic N-waves, and random variations in rise time. Effects of atmospheric turbulence are well beyond the capability of geometrical acoustics.

These phenomena raise interest in terms of how they can be dealt with, and also whether they require to be dealt with. For example, hypersonic F-function analysis is clearly necessary if that type of vehicle is to be considered, but the importance of shock rise time structure depends on the open question of which psychoacoustic response metric is appropriate for sonic boom. In the next section, each of these phenomena (as well as the elements of standard theory) is reviewed from its physical aspects.

3. Sonic Boom Theory

Linearized Supersonic Flow

Consider a slender axisymmetric body in uniform supersonic flow, with coordinates as illustrated in Figure 4. There will be a cylindrical acoustical wave with overpressure $\delta p = p - p_o$ given by:

$$\delta p(x-\beta r, r) = p_o \frac{\gamma M^2 F(x-\beta r)}{(2\beta r)^{1/2}} \tag{1}$$

where p = pressure
p_o = undisturbed ambient pressure
x = axial coordinate (body fixed)
r = radius
γ = ratio of specific heats
M = Mach number
$\beta = \sqrt{M^2-1}$ = Prandtl-Glauert factor

and

$$F(x) = \frac{1}{2\pi} \int_o^x \frac{A''(\xi)}{(x-\xi)^{1/2}} \, d\xi \tag{2}$$

where A is the cross-sectional area of the body as measured by the normal projections of cuts along planes aligned with the Mach angle, i.e., cuts along the x-βr lines in Figure 4. The quantity F(x) was introduced by Whitham,[5,12] and is generally referred to as the Whitham F-function. The F-function has an implicit dependence on Mach number due to A being defined by Mach tangent cutting planes, so that Mach number dependence is not limited to the explicit parameters in Equation (1).

Equations (1) and (2) follow from linearized supersonic flow theory[9] and the transonic[13] and supersonic[10,11] area rules. Lomax[14] showed that the axisymmetric body area rule could be generalized to asymmetric bodies, including the effects of lift, by generalizing A(x) to an equivalent area $A_e(x,\theta)$ which is a function of azimuthal angle θ about an axis through the body and defined by the flight direction. Walkden[15] applied this wave drag analysis to sonic booms. The equivalent area consists of two components: a volume component and a lift component. The volume component is calculated in the same way as for an axisymmetric body, except that the cutting plane must be aligned with the azimuth, such that it is tangent to that azimuth on the corresponding Mach cone. (Reference 7 has a good illustration of this.) The lift component of the equivalent area is given by:

$$A_L(x,\theta) = \frac{\beta}{\rho u_\infty^2} \int_0^x L(x,\theta)\, dx \tag{3}$$

where $L(x,\theta)$ is the component of lift per unit length, at axial station x, in the θ direction, and ρ is the ambient density. If the net lift normal to the wings is given by L(x), then $L(x,\theta)$ has a simple $\cos\theta$ dependence. The total lift of the aircraft equals the integral of L(x) along its length.

Calculation of the F-function requires A_e and evaluation of the integral in Equation (2). The integral is straightforward to evaluate for polynomials. In general, except for nominal idealized shapes, A_e for a given vehicle would be available in numerical form along an axial grid, for which it is natural to use some type of polynomial fit over each interval. This leads to a summation of closed form integrations over all intervals. In Reference 16, a procedure is given which uses parabolas, matching the slope at each mesh point. More recently, Reference 17 contains derivations of closed form solutions for higher order polynomials, and exposition of the summation formulae.

When representing an area distribution by a set of interval fits, it is important to pay attention to continuity of slope between intervals. A discontinuity in slope will cause A'' to be singular. This singularity has the form of a delta function, for which, as shown in Reference 7, there is a finite (and easily computed) contribution. The numeric calculation must either match slopes between intervals or include this contribution. It is particularly important to account for such a contribution at the nose of a vehicle.

It should be noted from Equation (2) that, far behind a body, F(x) has an asymptotic $1/\sqrt{x}$ behavior. A finite body has an infinite signature; this feature is included in the sketches of Figures 1 and 2. To achieve a finite signature, it is necessary have an infinite afterbody shaped such that it generates the complement of the asymptotic tail. This relationship is inherent in the axisymmetric linearized flow equations,. Its practical significance is that the F-function calculation must be carried out over a length greater than that of the body. Reference 17 contains a discussion of some practical numerical precision considerations involved when handling the asymptotic tails of a set of polynomial intervals.

When establishing the equivalent area, it is important that this area correspond to the shape of streamlines passing over the body. The effect of the propulsion system must be accounted for. The effective cross-section of air ingested by an air-breathing propulsion system must be subtracted from the cross-sectional area around the inlets. The exhaust plume must be accounted for as an effective afterbody. An extreme example of the importance of the propulsion system is in the sonic boom of launch vehicles, where highly underexpanded rocket exhaust plumes act as effective afterbodies which dominate the sonic boom characteristics of

the vehicle.[18,19] Aircraft propulsion systems generally are not as highly underexpanded, but their effect must be accounted for.

Geometrical Acoustics and Ray Tracing

The wave field given by Equation (1) is that of an axisymmetric wave. Locally, the wave behaves as a plane wave, with the cylindrical geometry entering via the $1/\sqrt{r}$ amplitude dependence. Spherical waves are similar, with a $1/r$ amplitude dependence. The general extension of this to a non-uniform medium is the method of geometrical acoustics, which applies when wavelength is small compared to other scale lengths. A full derivation of geometrical acoustics, including motion of the medium, was presented by Blokhintzev.[20] A very tidy presentation for a stationary medium was presented by Officer.[21] The review in this paper follow's Officer's format, and quotes Blokhintzev's final results for a moving medium. Another noteworthy derivation is that of Keller,[22] which is of particular interest for sonic boom since it considers a wavelength corresponding to the thickness of a shock wave, rather than the wavelength of of a continuous tone.

Consider propagation through an atmosphere with variable ambient sound speed and density, with no mean velocity and neglecting gravitational buoyancy. The wave equation is:

$$\frac{\partial^2 p}{\partial t^2} - \rho_o a_o^2 \vec{\nabla} \cdot \frac{1}{\rho_o} \vec{\nabla} p = 0 \tag{4}$$

where p now refers to the acoustic overpressure. A somewhat more complex equation applies if gravitational gradients or winds exist; terms explicitly involving acoustic density and velocity fluctuations also appear.

A solution is sought which is comprised of harmonic components of the form:

$$p(x,y,z,t) = P(x,y,z)\, e^{i\omega\left[t - \frac{W(x,y,z)}{a_\infty}\right]} \tag{5}$$

where ω = frequency
a_∞ = fixed reference sound speed
$P(x,y,z)$ = amplitude function
$W(x,y,z)$ = wavefront function

The wavefront function is a generalization of $x - \beta r$ in earlier discussions, and the amplitude function is a generalization of $1/\sqrt{r}$ in the axisymmetric solution. If Equation (5) is substituted into Equation (4), the following two relations (real and imaginary parts) are obtained:

$$1 - \frac{a_o^2}{a_\infty^2}(\nabla W)^2 = \frac{a_o^2}{\omega^2}\left(\frac{\vec{\nabla}\rho_o}{\rho_o} \cdot \frac{\vec{\nabla} P}{P} - \frac{\nabla^2 P}{P}\right) \tag{6}$$

$$\nabla^2 W + \vec{\nabla} W \cdot \left(2\frac{\vec{\nabla} P}{P} - \frac{\vec{\nabla}\rho_o}{\rho_o}\right) = 0 \tag{7}$$

If gravitational terms are included, there are additional terms $O(1/\omega^2)$ on the right-hand side of both equations. If wind is included, the left-hand sides are also slightly more complicated.

The terms on the right-hand side of Equation (6) (and Equation (7) in the more general cases) are of order $(\lambda/L)^2$, where λ is the wavelength of the acoustic signal and L is the scale length of atmospheric gradients and amplitude changes. If $\lambda \ll L$, the short wavelength limit, Equation (6) becomes:

$$1 - \frac{a_o^2}{a_\infty^2}(\nabla W)^2 = 0 \tag{8}$$

Equation (8) is the eiconal equation, familiar from geometrical optics, and states that the gradient of W is proportional to the local index of refraction. Propagation of sound is along geometrical rays orthogonal to wavefronts W.

Once the ray field is calculated, $\vec{\nabla} W$ may be written $\frac{a_\infty}{a_o}\hat{n}$, where $\hat{n}$ is the unit vector field representing ray direction. Equation (7) may be written as:

$$\vec{\nabla} \cdot \left(\hat{n} \frac{P^2}{\rho_o a_o} \right) = 0 \tag{9}$$

which has the obvious form of a continuity equation. The quantity $P^2/\rho_o a_o$ is proportional to the acoustic energy flux of a locally plane wave, so Equation (9) is simply conservation of energy. Defining a ray tube as a bundle of rays (analogous to a fluid dynamic stream tube), Equation (9) integrates to:

$$P\left(\frac{S}{\rho_o a_o}\right)^{1/2} = \text{constant} \tag{10}$$

where S is the ray tube area.

When wind is present, the ray acoustic equations are somewhat more complex. Because of convection, rays do not necessarily coincide with wave normals. The derivation is considerably longer, but the final results for the eiconal and amplitude equations are:[20]

$$q^2 - \frac{a_o^2}{a_\infty^2}(\nabla W)^2 = 0 \tag{11}$$

$$\vec{\nabla} \cdot \left[\left(\hat{n} + \frac{\vec{u}_o}{a_o} \right) \frac{P^2}{q\, \rho_o a_o} \right] = 0 \tag{12}$$

where $q = \left(1 + \frac{\vec{u}_o}{a_o} \cdot \hat{n}\right)^{-1}$

u_o = ambient wind speed

Equation (12) integrates to:

$$\frac{P^2}{q^2 \rho_o a_o} S = \text{constant} \tag{13}$$

along a ray tube defined by ray trajectories:

$$\vec{c} = a_o \hat{n} + \vec{u}_o \tag{14}$$

The ray tube area S is cut normal to rays c. The constant quantity defined by Equation (13) is sometimes referred to as the Blokhintzev invariant.

Calculation of rays and ray tube areas is a major task in sonic boom computer programs. Because geometrical acoustics is used to extrapolate an axisymmetric near-field solution, the initial rays forming the tube should be selected to match that structure. Typically, four rays are selected, separated by a time increment and an azimuthal increment, as illustrated in Figure 5. The initial directions of these rays are governed by the aircraft flight parameters and the azimuth. With that initial condition, ray shapes may be traced. The computer program described in Reference 23 traces rays by a direct numerical integration of the eiconal. All four rays are traced in this way, and ray tube areas computed by numeric differencing.

A more sophisticated approach is taken in Reference 6. An analytical derivation of the ray shape is performed for an arbitrary horizontally stratified atmosphere with winds. The result is an integral which must be evaluated numerically. The integral is, however, amenable to the following analysis leading to a ray tube area. The time along the aircraft trajectory and the azimuth define a particular ray whose shape may be described by horizontal coordinates x and y as a function of vertical coordinate z:

$$\begin{aligned} x(z) &= X(t, \theta, z) \\ y(z) &= Y(t, \theta, z) \end{aligned} \tag{14}$$

The four rays whose origins are sketched in Figure 5 are given by Equations (14) with the appropriate values of t and θ. The area S_H of a horizontal cut through the ray tube is given by the Jacobian at constant z of this system:

$$S_H = \frac{\partial(X, Y)}{\partial(t, \theta)} \tag{15}$$

The actual normal ray tube area S is this quantity times the cosine of the ray angle. The only drawback to this formulation is that S_H is singular at places where rays are horizontal, even though S may not be. A relaxation of this condition was obtained by Taylor,[24] who wrote the Jacobian in terms of a coordinate transverse to the ray direction.

A final detail of the propagation calculation is that sonic booms reaching the ground will be reflected. A receiver above the ground will see a complex boom consisting of direct and reflected signatures. At the ground, the boom will have the shape of the direct signature, but will be enhanced. Ground reflection coefficients are usually close to unity, resulting in pressure doubling.

Basic Sonic Boom Ray Acoustic Patterns

For steady flight in a uniform atmosphere, the wave and ray patterns form cones, as discussed earlier. These are sketched in Figure 6. The wave cone (or Mach cone) opens to the rear and represents the boom as it exists at a given instant. The ray cone opens forward and represents the space which will be traced out by the boom generated at that instant. Subsequent maneuvers will not alter the ray cone once it is generated. The ground intercepts of both cones, in level flight, are hyperbolas. Diving at an angle greater than the Mach angle causes the ray cone ground intercept to be an ellipse.

Wind and sound speed gradients distort the ray and wave cones. Rays in the troposphere are generally concave upward. This is shown in Figure 7, for views parallel to the flight track (Figure 7a) and across the track (Figure 7b). Note from the cross-sectional sketch that the upward curvature causes the boom footprint (or "carpet") to have a finite width, with a boomless geometrical shadow zone beyond. The upward curvature of the rays causes them to diverge laterally, while under the flight track they converge. Convergence is generally the stronger effect, particularly at low Mach number. Refraction tends to be less important at high Mach number, where rays are generally closer to vertical. Note that, for steady level flight, the rays generated at time $t + \Delta t$ are parallel to those generated at t. For a maneuvering aircraft, the initial directions of the rays are based on time-varying aircraft direction and Mach number, and are usually not parallel.

Figure 8 shows a case of interest, sonic cutoff for supersonic level flight at speed below ground elevation sound speed. The boom refracts upward and never reaches the ground. This situation is often cited as an example of boomless supersonic flight, but is of such a restricted range ($M < 1.15$ for stratospheric flight in the standard atmosphere) so as to be of little practical value. The point where rays turn upward also corresponds to a focus, which will be discussed in detail later.

Figure 9 shows the path of a sonic boom ray above the aircraft. It eventually is refracted downward in the thermosphere (passing through a focus, analogous to that at sonic cutoff) and reaches the ground as an "over-the-top" boom. Such booms exist,[25,26,27] but are of such low amplitude that they are of little real importance. Ones which are of audible amplitude[27] tend to be off-track and associated with particular high-altitude wind conditions, and not the simple ray patterns shown in Figure 9.

Nonlinear Steepening: Whitham's Rule

The concept of Whitham's rule has been stated earlier: the linear acoustic amplitude is correct to first order and must be applied to the propagation speed to obtain a uniformly correct far-field wave pattern. This section of the review follows the analysis used by Whitham in Reference 12, but with the linear solution written (as Whitham suggested) in a general geometrical acoustic form rather than plane, cylindrical, or plane waves in a uniform medium.

The acoustic overpressure, in ray-fixed coordinates, may be written:

$$\frac{p - p_o}{p_o} = \frac{F(\tau)}{\sqrt{B}} \qquad (16)$$

where

$$\tau = t - \int_0^s ds / a_0$$

t = time
s = distance along a ray
a_0 = undisturbed ambient sound speed

and B is an amplitude expression based on the Blokhintzev invariant, Equation (10) or (13). For simplicity, τ here corresponds to the windless form.

Whitham's rule calls for replacing a_0 in the expression for τ by $a + u$, the perturbed sound speed plus the velocity perturbation u. The normalized perturbations $(a - a_0)/a_0$ and u/a_0 are both proportional to $(p - p_0)/p_0$. For an isentropic acoustic wave the propagation speed is:

$$a + u = a_0\left(1 + \frac{\gamma + 1}{2\gamma}\frac{p - p_0}{p_0}\right) \tag{17}$$

The parameter τ represents a point on the acoustic wave, and t is its arrival time at location s. Using Equation (17), the arrival time, to first order, is:

$$t = \tau + \int_0^s \frac{ds}{a_0} - \frac{\gamma + 1}{2\gamma a_h} F(\tau) \int_0^s \frac{ds}{\sqrt{B}} \tag{18}$$

Equation (18) has been written in terms of t, rather than τ, so as to present an explicit relationship.

Equation (18) is the quantification of the process described earlier and illustrated by Figures 3b to 3c. Note that the advance of each signature point (the last term of Equation (18)) is proportional to its F-function value and a quadrature which is independent of F. The quadrature term is part of the ray geometry solution and, in various normalized forms, has been denoted the age parameter[6] or the advance factor.[28]

Parts of the aged signature constructed in Figure 3c are triple valued. This is physically impossible. At some earlier time, the aging process would cause the signature slope to be vertical, at which point there would be a discontinuous pressure jump. Propagation of this jump must be handled as a shock wave, rather than an isentropic wave. Linearizing the Rankine-Hugoniot relations gives the following speed for a weak shock of strength Δp:

$$u_s = a_0\left(1 + \frac{\gamma + 1}{4\gamma}\frac{\Delta p}{p_0}\right) \tag{19}$$

This is slower than the isentropic wave speed behind it, so that the original signature is absorbed into the shock. The shocks are sketched in Figure 3. In general, the linearized shock speed is equal to the average of the isentropic wave speeds ahead of and behind it. This leads to the "area balancing" rule for fitting shocks: construct the steepened isentropic signature, then eliminate triple-valued areas by fitting shocks such that total area is conserved. In Figure 3, the shaded areas ahead of and behind each shock are equal.

Signature aging will eventually lead to an N-wave. Key quantities for an N-wave are the shock overpressure and the total duration. Concentrating on the forward, positive-

overpressure portion of the N-wave, these are obtained by determining the value of τ corresponding to the wave just behind the shock. This value of τ will increase with distance from the aircraft, as earlier phases of the wave are absorbed into the shock. Denoting this value of τ as T(s), the arrival time of the shock may be written, from Equation (18), as:

$$t_{shock} = T(s) + \int_0^s \frac{ds}{a_o} - \frac{\gamma + 1}{2\gamma a_h} F(T(s)) \int_0^s \frac{ds}{\sqrt{B}} \tag{20}$$

If Equation (20) is differentiated once with respect to s, it gives dt_{shock}/ds, which is the reciprocal of the shock speed u_{shock} given in Equation (19). These two equations may be combined, giving a differential equation for T(s). Manipulation of this equation is presented in Reference 12 and yields F(T(s)):

$$F(T(s)) = \left[2 \int_0^{T(s)} F(\tau)\, d\tau\right]^{1/2} \left[\frac{\gamma + 1}{2\gamma\, a_h} \int_0^s \frac{ds}{\sqrt{B}}\right]^{-1/2} \tag{21}$$

This is an implicit relation, since T appears as a limit in one integral on the right-hand side. At very large distances, most of the original F-function will be engulfed in the shock, and T(s) will be sufficiently close to the first zero of F at τ_o that the integral will asymptote $\int_0^{\tau_o} F(\tau)\, d\tau$. The final shock strength is:

$$\Delta p_{shock} \sim \frac{p_o}{\sqrt{B}} \left[2 \int_0^{\tau_o} F(\tau)\, d(\tau)\right]^{1/2} \left[\frac{\gamma + 1}{2\gamma\, a_h} \int_0^s \frac{ds}{\sqrt{B}}\right]^{-1/2} \tag{22}$$

For plane (B = constant), cylindrical (B α s), and spherical (B α s^2) waves in a uniform atmosphere, the overpressure is:

$$\Delta p_{shock} \quad \alpha \quad \begin{cases} s^{-1/2} & \text{plane} \\ s^{-3/4} & \text{cylindrical} \\ s^{-1} (\log s)^{-1/2} & \text{spherical} \end{cases} \tag{23}$$

and the duration (by combining Equations (18) and (21)) is:

$$\Delta t \quad \alpha \quad \begin{cases} s^{1/2} & \text{plane} \\ s^{1/4} & \text{cylindrical} \\ (\log s)^{1/2} & \text{spherical} \end{cases} \tag{24}$$

Two points should be noted regarding the N-wave solution and Equations (22) and (23). First, this is a far-field solution. At distances where a pure N-wave has not evolved (or is not an acceptable approximation), Equation (18) and the construction of Figure 3 must be used. This is a real consideration for large aircraft (such as SSTs) where typical conditions are such that mid-field signatures are expected at the ground.[29] Second, not all pulses will be represented by Equations (23) and (24) in the far field. There is an assumption that $F'(\tau)$ is constant near τ_o.

For some types of blast waves, modeled as a shock and decaying exponential, this assumption does not apply and different far-field laws can be derived.

Implementation of Standard Theory

The discussion thus far has covered the essentials of standard boom theory. A complete implementation of this theory (particularly ray tracing in a real atmosphere) is sufficiently complex that a computer is required, and a number of programs have been written. These programs generally treat the F-function as an input and perform the ray tracing and signature aging calculations. The F-function input can be supplied from a separate linearized flow calculation, from wind tunnel data, or from computational schemes which will be discussed later in this paper. Three such programs are publicly available.

The first computer program to handle all details for a general maneuvering vehicle in a horizontally stratified atmosphere with winds was due to Hayes *et al.*,[6] and is commonly referred to as the ARAP model. Ray tracing details of the program have been discussed previously. Signature aging and shock fitting are treated by a numeric implementation of the procedure sketched in Figure 3. With the publication of this program, standard sonic boom predictions could be declared to be a solved problem.

A second, equivalent, program in wide use is that developed by Thomas.[23] This program is structured to accept near-field signature input in the form of pressure versus distance wind tunnel data. It uses a purely numeric ray tracing technique, noted earlier, and handles signature evolution by the "waveform parameter" technique. With the waveform parameter technique, the signature is divided into piecewise linear segments, and evolution handled in closed form by a generalization of the analysis outlined here as Equations (19) through (21). This algorithm is applied at each mesh point in the ray tracing.

The third available program is the TRAPS model.[24] This is a new code based on the ARAP formulation. It was developed for analysis of over-the-top booms as sketched in Figure 9 and has the capability to trace rays through horizontal segments. It also has a simple method to estimate the amplitudes of booms which have passed through a focal zone (often the case when rays become horizontal), although it cannot predict signatures near a focus.

Several other sonic boom programs are in use but not yet publicly available. These tend to be variations (sometimes major variations) of either the ARAP or Thomas models and tend to be project oriented. It is expected that some of these will be made publicly available in generic form in the near future. It is worth noting that, while sonic boom computer programs were originally written for mainframe computers, they are within the capabilities of current personal computers, and that is the target for current software.

Sonic boom resulting from steady rectilinear flight in a standard atmosphere is simple enough that a full computer calculation is not always necessary. In particular, once the ray tracing and age parameter calculations have been performed, they can be applied to any near-field signature at the same flight conditions. In Reference 28, charts of normalized ray tube area, acoustic impedance, and advance factor are presented for rays under the flight track over a range of altitudes and Mach numbers. This provides the information to manually implement the construction sketched in Figure 3.

A more general handbook procedure was developed by Carlson.[30] That scheme is applicable to booms where the ground signature is expected to be an N-wave. It utilizes the cylindrical scaling relations shown in Equations (23) and (24), plus charts of adjustment factors for atmospheric effects and type of aircraft. The charts were developed from fits to a large number of full ray tracing calculations and F-function calculations for various types of

large number of full ray tracing calculations and F-function calculations for various types of aircraft. The procedure allows calculation of the boom ground impingement point (off-track as well as on-track), lateral cutoff distance, and N-wave overpressure and duration. A byproduct of the procedure is a method to compute an N-wave approximation to the F-function. This approximate F-function can be used as input to a full computer model, and is appropriate when it is known that a far-field N-wave will occur but it is necessary to compute boom ground patterns for a particular maneuver or non-standard atmospheric condition.

Hypersonic Vehicles

Standard theory has been well validated by numerous flight tests. References 31 to 33, which cover altitudes from 10,000 feet to 75,000 feet, Mach numbers from 1.1 to 3.0, and aircraft types from small fighters to large bombers, exemplify this. A few data points are available for the X-15 at Mach number up to 4.8 and altitude of 70,000 feet.[34] The X-15 data agree well with predictions from a simplified model similar to Reference 30, but the effect of the near-field flow is estimated rather than calculated from slender body theory.

Wind tunnel tests, exemplified by References 35-39, have validated both near- and far-field theory for models ranging from flat plates and bodies of revolution to complex aircraft, at Mach numbers up to about 2. At Mach numbers above about Mach 2.5 to 3.0, and at high lift coefficients, wind tunnel tests reported in References 40 and 41 exhibit departure from the near-field Whitham-Walkden slender body area rule theory. Above Mach 3, slender-body theory does not provide reliable results.

If required, F-functions can be obtained from wind tunnel measurements. This has been done for launch and reentry vehicles,[42,43] with very good agreement with flight measurements.[44] Computational fluid dynamics has come to be regarded in some ways as an alternative to wind tunnel testing, and CFD calculations of selected points has shown good agreement with wind tunnel data.[43,45] Calculation of a complete F-function from CFD requires a spatial grid much larger than normally used for aerodynamic design purposes, and poses questions of practicality with current computers and codes. (It is possible that at some time in the future computational power will increase to the point where the entire flow field of any vehicle can be computed to arbitrarily large distance, at which time most of the contents of this paper will be a curious antiquity.)

Currently, there is one analytic model for sonic boom at hypersonic speeds. It is based on a concept by Seebass[46] that all hypersonic bodies have effectively blunt noses (both physical blunting, such as reentry vehicles, and aerodynamically because of the entropy layer on slender vehicles), and the resultant drag dominates the sonic boom. Such a vehicle is equivalent to a spherical nose on a slender infinite afterbody. The far-field wave pattern can be computed by means of a blast wave analogy. Tiegerman[47] performed a careful analysis of this configuration, identifying the significant terms in the hypersonic flow equations, writing the appropriate similitude/scaling laws, and matching near-field flow (where entropy layer effects are important) to the far field, where geometrical acoustics and Whitham's rule apply. Quantitative results for the far field were obtained, incorporating constants from a numerical solution of the equivalent blast wave. The analogy is valid for the positive-pressure phase of the far-field N-wave and also provides an estimate of the location of the trailing shock. The final far-field sonic boom results were combined with geometrical acoustics atmospheric corrections for an isothermal model atmosphere. The results for the N-wave overpressure, positive phase impulse I, and duration T are:

$$\Delta p = 0.59 \frac{P_g^{5/8} D^{3/8} \exp(-h/8H)}{H^{1/4} h^{1/2}} \tag{25}$$

$$I = 0.16 \frac{P_g^{1/4} D^{3/4} \exp(h/4H)}{h^{1/2} a_g} \tag{26}$$

$$T = 1.08 \frac{P_g^{-3/8} D^{3/8} \exp(3h/8H) H^{1/4}}{a_g} \tag{27}$$

where P_g = ambient pressure at ground

a_g = ambient sound speed at ground

D = vehicle drag

H = atmospheric scale height

h = flight altitude

Calculations from this theory agreed well with available data from Apollo 15 and 16 reentry. Flight Mach numbers were from 4.6 to 15.6, and the Apollo vehicle clearly matches the postulated model.

It is interesting to examine Tiegerman's results for aircraft configurations. Figure 10 (adapted from Reference 48) shows the overpressure and positive-phase impulse as a function of altitude. Shown for comparison are the same quantities for a nominal 400,000-pound SST at Mach 2.7, calculated from Carlson's simplified model.[30] The SST boom is significantly greater than the hypersonic drag-dominated boom. This type of comparison has led to the speculation that a hypersonic transport may have a sonic boom advantage. However, there are two points to consider. First, the hypersonic theory is effectively a volume-only model and does not account for vehicle lift. Almost 40 percent of the example SST boom is due to lift. An extension of the theory to account for lift-induced boom would be useful. Second, the drag-dominated theory implicitly assumes a short body. This assumption results in durations considerably shorter than those calculated for the SST, with a considerably shorter impulse. A phenomenon related to the short duration is that as a short pulse ages, its amplitude decays more rapidly than a long pulse. This behavior (which is a key element in sonic boom minimization analyses[48,49]) causes the shock overpressure itself to be lower.

The Tiegerman/Seebass hypersonic boom theory clearly provides valid results for true blunt bodies at high Mach numbers. The open question is how to obtain an F-function for slender bodies at Mach numbers below this asymptotic limit but above the linear flow regime. Direct CFD calculations appear to be one route for the future, but CFD calculation are somewhat like wind tunnel data in that one cannot easily tinker with the results for design iteration purposes. The approach of Tiegerman and Seebass has proven itself to be valid at one extreme, however, and it would be very gratifying if it could be extended to the high-speed aircraft regime.

Extreme Near-Field F-functions

A topic related to hypersonic F-functions is the use of near-field data, either from wind tunnel tests or from CFD calculations. The F-function and the starting point for geometrical acoustic calculation must begin at a radius where amplitudes are at linear acoustic levels, and also where the assumption of local axisymmetric flow is valid. Even where linearized flow applies, a region close to a lifting body will have significant cross-flow. One computational method has been developed to handle this extrapolation. The method is the Modified Method of Characteristic (MMOC).[50,51] MMOC uses the three-dimensional method of characteristics to account for cross-flow. It is denoted "modified" because the locations of characteristics are adjusted to first order, according to Whitham's rule, so as to make it appropriate for large-radius extrapolation of sonic booms. The characteristic relationships employed are valid in a plane of symmetry, and the formulation allows atmospheric gradients compatible with geometrical acoustics. The program is suitable for extrapolation of near-field (i.e., crossflow important but acoustical amplitude) wind tunnel data under an aircraft to predict on-track sonic boom for steady level flight.

Focal Zones

Under certain conditions, converging ray patterns can exist which produce foci, where ray tube area is zero and the geometrical acoustics solution is singular. Intuitively, one thinks of lens-like focusing and cylindrical implosions. Calculations[52] and laboratory measurements[53] of implosions of initially weak waves exhibit substantial amplifications. This has led to concern over the existence and amplitude of focused "superbooms". However, sonic boom focal zones tend to be of lower order types, with moderate amplification.

Figure 11 illustrates one type of sonic boom focus, that due to linear acceleration. As Mach number increases the Mach angle decreases and rays converge to a focal point. The effective focal length of this is related to dx/dt and inversely to $d\mu/dM$. If the aircraft accelerates at a constant rate, $d\mu/dM$ decreases while dx/dt increases, so that the focal length will increase. The focus is thus smeared out along the caustic line shown in Figure 11. The focus at any point along the caustic represents focusing of an infinitesimal portion of the wavefront. The caustic forms a boundary, or envelope, of the wave field, and is tangent to the rays it bounds. In three dimensions, the caustic is a two-dimensional surface. The situation sketched in Figure 11 shows that a focus will always exist at the edge of the supersonic region when an aircraft accelerates to supersonic speeds. Focal zones are thus not rare in number, since there is one at the edge of every boom, but are rare in that the area involved is very small compared to the total area of a boom footprint.

A caustic surface can also exist due to atmospheric refraction. The sonic cutoff line in Figure 8 is a caustic, and a similar caustic exists at the vertical turning point in the "over-the-top" boom shown in Figure 9. For a maneuvering aircraft in the real atmosphere, caustic surface geometries can be quite complex. Reference 54 presents the results of an extensive series of focal zone flight tests, and has examples of caustic and focusing ray geometries for accelerations and turns. Reference 55 is a study of focusing ray geometries, and has additional illustrations. References 56 and 57 contain sketches of focus geometries, and a discussion of the fact that the there are several kinds of focus, with the "smooth caustic" shown in Figures 8, 9, and 11 being the simplest and weakest kind.

The fact that the caustic forms an edge to the wave field indicates that there is a lateral scale not considered when applying geometrical acoustics, and diffraction should play a role in limiting the singular geometric behavior. This focal zone behavior occurs in a narrow region near the caustic, and it is appropriate to examine this region in local coordinates. Consider coordinates X, Y parallel and normal to the caustic at the caustic/ray tangent point. The ray

shape in some small region is given by $Y = X^2/2R$, where R is the relative curvature between caustic and ray. The geometric ray tube area is proportional to $\sqrt{RY}$, and geometric signature strength follows a $Y^{-1/4}$ relation. A linear acoustic solution which can be represented in these coordinates is contained in Reference 58. Diffraction effects in that analysis reduce the order of the singularity.

Nonlinear effects are considered to be important for focused sonic booms. Whitham[12] suggested that amplitude increases associated with focusing would cause a converging wavefront to straighten and thus never actually focus. This assertion did not turn out to be the case in general, but the effect does partially occur and nonlinearity plays a role in further limiting the singularity. The appropriate governing equations were set down by Guiraud,[59] who also derived a scaling law for a focused weak shock wave. Derivation of Guiraud's similitude and scaling law have been reiterated by Gill and Seebass[60] and Gill[61] in their development of a numerical focus solution, and the following discussion uses their notation.

Near a caustic, the governing equation is the nonlinear Tricomi equation:

$$\left[\frac{Y}{R} + \frac{2\Gamma}{U}\Phi_X\right]\Phi_{XX} - \Phi_{YY} = 0 \tag{28}$$

where Φ = velocity potential
U = flow velocity = sound speed at $Y = 0$
$\Gamma = \gamma + 1$

The caustic surface is at $Y = 0$. The Y/R term in Equation (28) represents the existence of a sound speed gradient such that $M^2(Y) = 1 + Y/R$. Rays tangent to the caustic at $Y = 0$ have radius of curvature R. The linear form of Equation (28) is hyperbolic for positive Y and elliptic for negative Y. This equation corresponds to the cutoff geometry of Figure 8, but the coordinates can be interpreted as the caustic-relative coordinates discussed earlier.

Equation (28) can be reduced to canonical form

$$(y + \phi_x)\,\phi_{xx} - \phi_{yy} = 0 \tag{29}$$

via the transformation

$$\begin{aligned} X &= Sx \\ Y &= Y^{1/3} S^{2/3} y \\ \Phi &= \frac{US^{5/3}}{2\Gamma R^{2/3}}\phi \end{aligned} \tag{30}$$

This system has linear characteristics $p,q = x \pm 2/3\, y^{3/2}$. The boundary condition is that the incoming wave satisfy $\phi_X(p) \sim \mu y^{-1/4} F(p)$, where $\mu = \Gamma A (R/S)^{7/12}$ is a measure of the incoming signal strength at distance S from the caustic. The dependence on μ (not to be confused with Mach angle) can be scaled out by the transformation:

$$x' = \mu^{6/5} x$$

$$y' = \mu^{4/5} y \qquad (31)$$

$$\phi' = \mu^{2} \phi$$

If a solution $\phi'_{x'}$ is obtained for the normalized canonical form, then the solution in physical coordinates is

$$\frac{C_p(X)}{C_p(p)} = -\frac{\phi'_{x'}}{\mu^{4/5}} \left[\frac{Y}{C_p(p) \Gamma R} \right]^{1/5} \qquad (32)$$

where C_p is the pressure coefficient and $C_p(p)$ corresponds to the incoming wave boundary condition. The scaling law derived by Guiraud applies to the maximum pressure associated with an incoming shock wave, and is:

$$\frac{C_{p_{max}}}{C_{p_{ref}}} = \text{constant} \cdot \left[\frac{Y_{ref}}{2 \Gamma R C_{p_{ref}}} \right]^{1/5} \qquad (33)$$

where $C_{p_{ref}}$ is the pressure coefficient at Y_{ref}. The constant is universal, and must be determined experimentally or numerically. Equation (32) is more general in that it provides scaling of the entire signature shape, provided that the shape taken as the incoming boundary condition is appropriate. Since the shock waves are often regarded as the most important part of a sonic boom signature, a solution for a unit step function would have great utility.

Such a solution has been computed by Gill and Seebass. Their calculation procedure was to first note that a linear solution could be constructed from hypergeometric functions. The effects of nonlinear behavior were then introduced via a coordinate strain, analogous to Whitham's rule. Numeric results were obtained for a range of Y values around the focus. Figure 12 shows the Gill-Seebass solution for the position corresponding to maximum shock amplification.

It is reasonable to estimate the shape of a focused N-wave by applying the Gill-Seebass shock solution to each shock wave. This approach was adopted in in the sonic boom prediction program described in References 56 and 57. At each shock wave, an overall amplification factor was computed (via the scaling law) corresponding to the peak. The difference between the Gill-Seebass shock solution and the initial step function is multiplied by that factor and added to the N-wave. Some judicious smoothing is applied to blend the focus signature at locations far from each shock. Figure 13 shows the resultant focused wave shape. This signature bears a very strong resemblance to measured focus boom signatures.[54,62] In Reference 56, it is shown that the predicted peak overpressures are in very good agreement with the flight test data of Reference 54 and with focus measurements made in a ballistic range.[63] It is also shown in Reference 56 that overpressures reported in Reference 54 just outside the focal zone exhibit the $Y^{-1/4}$ behavior expected from the caustic/ray geometry and required by the boundary condition to the Tricomi equation.

The Gill-Seebass analysis does not necessarily represent the ultimate mathematical solution at a focus. Reference 64, for example, points out an inconsistency in shock fitting

boundary conditions associated with the nonlinear coordinate transformation. That does not appear to be fatal, but rather the kind of detail problem associated with practical approximations, and estimates of its consequences are small.[56,60] A more recent analysis of a shock at a caustic[65] yields results consistent with the Gill-Seebass result. This is, however, an area which should be studied further.

Analysis of focal zones has tended to concentrate on the maximum-shock signature at the caustic. Other parts of the focal zone are of interest. Figure 14, taken from Reference 62, is a sketch of the incident and reflected waves at a caustic and the types of signatures observed. The incident wave is an N-wave. The reflected wave has a U-shaped signature. The maximum focused signature is similar to Figure 13 and appears to be somewhat of a transition between the incident N- and reflected U-waves. Below the caustic, there is a decaying sine-like evanescent wave. All three types of waves have been measured in Reference 62 and in other (as yet unpublished) studies. Reference 66 contains an acoustic analysis of these signatures. The TRAPS computer program[24] uses a Hilbert transform to approximate the nature of the reflected U-wave far from the focus, a detail of some importance for over-the-top booms. A consistent nonlinear analysis of all three regions would be very desirable.

A higher order type of focus which can occur is associated with a two-sheet caustic forming a cusp. A cusped caustic can be generated by a transient maneuver such as turn entry. Measurements of such a cusped "superfocus" are reported in Reference 54, with a shock amplitude about twice that of the adjacent smooth caustic focus. The governing equations and scaling law for a cusped caustic have been written,[67,68] but to date no numerical results comparable to References 60, 61, and 65 have been obtained.

Atmospheric Turbulence Effects

Figure 15 shows typical measured sonic booms from one aircraft under calm and turbulent atmospheric conditions.[69] Three phenomena are apparent. First, the sonic booms measured under turbulent conditions have considerable fine structure superposed on the basic N waves. There is a variability in peak overpressure, primarily associated with particular positive or negative spikes. Distortion is similar about both shocks of a given boom, and tends to be strongest immediately behind the shocks. Second, rise times are clearly longer than the assumed zero-thickness jumps, and are longer than would be expected from viscous absorption calculations. Third, rise times under turbulent conditions are longer than under calm conditions, and exhibit significant variability, although the front and rear shocks of a given N-wave are similar.

These phenomena are associated with turbulence in the lowest several thousand feet of the atmosphere. References 70 and 71 contain reviews of the empirical data base and interpretations of these phenomena. In this paper, the key theoretical models are reviewed. Because this is a rather specialized area, the theories are described but the governing equations are not presented.

The crux of distortion of sonic booms is scattering by turbulence. When performing scattering analysis, the wave equation is written for a non-homogeneous medium, with turbulence represented as a small variation about the mean. A solution is sought which is in the form of an expansion, with turbulence amplitude being the expansion parameter. The zero'th order solution is the solution to the homogeneous wave equation for the mean media properties. This is followed by a sequence of inhomogeneous wave equations, where the left-hand side represents the next order in the solution and the right-hand side consists of source terms associated with the interaction of turbulence with the previous lower order solution. Key expositions of scattering analysis, as it was performed in the 1960s, are contained in the books by Chernov[72] and Tatarski.[73] The perturbation expansion nature of scattering theory is

discussed by Keller.[74] An important concept in these scattering formulations is that of frozen turbulence, where the time scale of turbulent structure changes is very slow compared to the propagation time through the medium. This simplifies the formulation time (derivatives of turbulence are neglected), and explains why turbulence effects are similar on both shocks of a given boom.

The scattering equations are generally written for a continuous pure tone, and scattered sound is generally treated as coming from the volume through which the sound has propagated. Scattering is stronger for high frequencies than for low. Crow[75] noted that high frequencies in a sonic boom are associated with the shocks, so that scattering should be associated with those and not a continuous wave. He wrote the scattering equations relative to the shock, much in the spirit of Keller's shock-based derivation of geometrical acoustics.[22] The scattered sound received at a given point is then associated with a "paraboloid of dependence", with the receiver point behind the shock being the focus and the shock being the directrix, rather than a three-dimensional volume. The distance behind the shock, rather than frequency, becomes a primary variable. Crow's final result was that the envelope of rms fluctuations behind each shock would follow a $(h/h_C)^{-7/12}$ dependence, where h is the distance behind the shock and h_C is a parameter related to the strength and structure of the turbulence. The result is singular at $h = 0$ for a zero-thickness shock, but application to a finite-thickness shock eliminates this singularity.[76,77] Crow's results are qualitatively very satisfactory, and appear to be of the correct magnitude for reasonable values of turbulence. The absence of turbulence measurements during any sonic boom flight tests has, however, precluded quantitative validation.

Shock Wave Rise Times

Crow speculated that shock thickening might be associated with energy scattered out of the shock. This concept was consistent with a second-order scattering analysis by Keller[74] which showed that long distance propagation through turbulence could result in an effective attenuation. Plotkin and George[78] and Plotkin[79] developed a shock structure model incorporating the turbulent scattering attenuation mechanism and first-order nonlinear steepening analogous to Whitham's rule. The result was a Burgers equation with an effective absorption coefficient dependent on turbulence amplitude and structure. This yielded a shock structure with thickness proportional to the effective absorption coefficient and inversely proportional to shock amplitude. The dependence on shock amplitude matched very well the trend of a wide range of sonic boom and weak blast wave data. The magnitude of predicted rise times agreed well for reasonable assumed turbulence, but the absence of turbulence data during sonic boom tests again precludes quantitative validation.

The scattering concept for rise times has some problems. First, it does not explain where the energy goes: the scattered perturbations do not have substantially higher frequency content than the shock wave. A corollary to this is that shocks have a finite rise time even under calm conditions. If some other mechanism is responsible for the basic calm condition rise time, then scattering could account for longer and variable rise times under turbulent conditions. Second, scattering analysis employs statistical techniques, including ensemble averaging, which must be carefully interpreted for any particular single event. This is discussed in Reference 70. Finally, the second scattering analysis is a long distance result. It is necessary to ascertain whether conditions are appropriate for the scattered energy to have been separated from the shock front. Reference 78 contains a detailed analysis of this, and shows that the distances and other parameters associated with sonic booms are indeed appropriate for this mechanism to apply.

An alternate theory of turbulence-induced rise time has been proposed by Pierce.[80] This is worth examining for its different perspective, which attempts to avoid some of the statistical problems noted above, but introduces others which may be more serious.

In addition to genuine considerations of the assumptions in the Plotkin-George and Pierce theories for turbulence-induced rise times, the role of turbulence in shock structure has been questioned by several specious studies. In Reference 81, a quantity is defined as a shock thickness which has no physical relation to shock thickness, but rather the overall frequency content of the pulse. Since neither turbulence model accounts for the ultimate loss of acoustic energy (just its spatial relocation), that quantity shows no effect. References 82 and 83 report attempts to measure turbulence-induced thickening. Both experiments involved propagation over distances of feet or tens of feet, rather than the thousands of feet encountered by sonic booms and required by theory. The resultant declarations that turbulence does not affect rise time are, at the very least, misleading.

Reference 83 is, however, quite valuable because its primary content was to report the latest in a series of studies to apply modern molecular-relaxation based absorption theory to shock waves. This theory, which has been well validated and accepted,[84] shows that atmospheric absorption of sound is several orders of magnitude larger than the viscous absorption mechanism which greatly underpredicted measured rise times. The magnitude of absorption depends on frequency and is also sensitive to temperature and humidity of the air. Reference 83 itself is not appropriate for sonic booms, since it involved higher amplitude artillery blasts over short distances. An earlier publication by Bass *et al.*[85] applied molecular absorption theory to weak shock waves, including a nominal sonic boom. Figure 16 shows rise times as a function of shock amplitude for the Plotkin-George turbulence theory (several values of turbulent attenuation coefficient), the molecular absorption theory,[85] classical viscous absorption, and measured sonic booms and blast waves. A nominal rise time is drawn through the data. All three theories have the correct slope, although the classical absorption theory clearly underpredicts. The turbulence theory brackets the measurements. Some of the molecular absorption calculations match the measurements, and overall tend to agree well with the lower edge of the measurements, which presumably correspond to calm conditions. It very much appears from this that molecular absorption is the base mechanism accounting for much of the shock structure, while the turbulence mechanism accounts for anomalously high and variable rise times observed under turbulent conditions. It also very much appears that this topic would greatly benefit from a unified analysis applied to flight test data which included turbulence, temperature, and humidity measurements.

4. Current Needs

As noted in the Introduction, there are three current applications of interest for sonic boom: an advanced SST, military air training operations, and atmospheric flight of spacecraft. The needs of each of these, beyond standard boom theory, are discussed below.

Advanced Supersonic Transport

Advances in aircraft technology suggest that sonic boom amplitudes for this type of aircraft, also referred to as a High Speed Civil Transport (HSCT) or the "Orient Express", could be made substantially lower than first generation SSTs, potentially to the point that overland flight could be acceptable. Minimization of sonic boom would then be a key design parameter. Studies of minimization[48,86,87,88] indicate that minimization is achieved, not through unique concepts or tricks, but through careful applications of certain principles to the overall aircraft design. It is necessary that sonic boom analysis be brought into the mainstream of the aircraft design process, rather than be a side calculation. The Whitham-Walkden area rule procedure is not adequate, for two reasons. First, aircraft are no longer designed by that level of technology:

modern CFD codes are used relatively early in the aerodynamic design process. Second, an advanced SST is likely to be designed for speeds above Mach 3, and/or have a blended wing/body configuration not amenable to linearized flow approximations. There is thus a need for a hypersonic boom generation methodology which is compatible with current aerodynamic design technology.

Another issue is focal zones. If an aircraft flies supersonically over land, the initial focus at the edge of the carpet would also be over land. Such focal zones are quite small (and may not cause impact more significant than unfocused booms),[89] and current prediction methodology probably provides adequate predictions. However, there are some uncertain aspects to currently available focus boom solutions, and resolution of such uncertainty is necessary to ensure confidence when such predictions are applied to environmental assessment.

A third important issue is atmosphere effects and rise times. The effect of variability must be understood at least to the point of assessing its effect on the average noise environment. Shock wave rise times, as noted earlier, can play an important role in loudness (and hence acceptability) calculations.

Air Combat Maneuver Training

Military air combat maneuver (ACM) training operations take place in specially designated airspaces and can involve brief supersonic events. Typically, supersonic flight occurs for only a few percent of total mission time. Individual supersonic events rarely last as long as 30 seconds,[57,89,90] and are almost never simple level flight. The focal zones associated with the edge of the boom carpet tend to be a major portion of the total footprint, simply because a carpet boom is never really established. Measurements of ACM booms tend to show wave patterns similar to those sketched in Figure 14: focus U-waves, incident N-waves combined with reflected U-waves, and evanescent sine waves. It is rare to observe simple steady flight N-waves. Estimates of the average boom environment require a better understanding of the entire caustic region. A unified theory for this region, as suggested earlier, would be highly desirable. Predictions based on steady cruise condition booms and maximum peak focus booms are likely to overstate the environment.

The aircraft and Mach numbers involved are such that steady cruise booms would be N-waves which are well predicted by standard theory. The theoretical gap is a complete description of the caustic region. Another problem is that, given the nature of air combat, the occurrence of supersonic events can be predicted only statistically. While that is a major issue in developing average environmental predictions, it is a data acquisition and system modeling problem, not a gap in sonic boom theory.

The issues of turbulence-induced variability and the effect of rise times also apply here, since the application is environmental assessment.

Atmospheric Flight of Spacecraft

During reentry, the space shuttle has supersonic flight phases which generate sonic booms over land. Similar operations would be expected for the National Aerospace Plane. The major shortcoming of standard boom theory is that these vehicles are hypersonic. Shuttle sonic booms have very successfully been made by using F-functions developed from wind tunnel measurements.[19,43,44] Those data were collected at Mach numbers up to 6. Predictions of sonic boom from higher Mach number flight regimes would require additional wind tunnel measurements. This is an area where a hypersonic F-function prediction theory would be of direct benefit. The National Aerospace Plane faces similar modeling problems.

REFERENCES

1. Gold, T., "The 'Double Bang' of Supersonic Aircraft", Nature, 170, p. 808, November 1952.

2. Warren, C.H.E., "Noise From Aircraft at Supersonic Speeds", Nature, 171, 214-216, January 1953.

3. Landau, L.D., "On Shock Waves at Large Distances From the Place of Their Origin", J.Phys.USSR, 9, 496, 1945.

4. DuMond, J.W.M., Cohen, E.R., Panofsky, W.K.H., and Deeds, E., "A Determination of the Wave Forms and Laws of Propagation and Dissipation of Ballistic Shock Waves", JASA, 18 (1), 97-118, 1946.

5. Whitham, G.B., "The Flow Pattern of a Supersonic Projectile", Communications on Pure and Applied Mathematics, 5, 301-348, 1952.

6. Hayes, W.D., Haefeli, R.C., and Kulsrud, H.E., "Sonic Boom Propagation in a Stratified Atmosphere, With Computer Program", NASA CR-1299, April 1969.

7. Seebass, A.R., "Sonic Boom Theory", J.Aircraft, 6 (3), 177-184, May-June 1969.

8. Runyan, L.J., and Kane, E.J., "Sonic Boom Literature Survey". "Volume I: State-of-the-Art", FAA-RD-73-129-I; "Volume II: Capsule Summaries", FAA-RD-73-129-II, September 1973.

9. Hayes, W.D., "Linearized Supersonic Flow", Thesis, California Institute of Technology; reprinted as North American Aviation Report AL-222; available as Princeton University AMS Report 852, 1947.

10. Jones, R.T., "Theory of Wing-Body Drag at Supersonic Speeds", NACA RM A53H18a, 1953.

11. Whitcomb, R.T., and Fischetti, T.L., "Development of a Supersonic Area Rule and an Application to the Design of a Wing-Body Combination Having High Lift-to-Drag Ratios", NASA RM L53H31a, 1953.

12. Whitham, G.B., "On the Propagation of Weak Shock Waves", J.Fluid Mech., 1, 290-318, 1956.

13. Whitcomb, R.T., "A Study of the Zero-Lift Drag-Rise Characteristics of Wing-Body Combinations Near the Speed of Sound", NACA RM L52H08, 1952.

14. Lomax, H., "The Wave Drag of Arbitrary Configurations in Linearized Flow as Determined by Areas and Forces in Oblique Planes", NACA RM A55A18, 1955.

15. Walkden, F., "The Shock Pattern of a Wing-Body Combination, Far From the Flight Path", Aeronautical Quarterly, IX (2), 164-194, 1958.

16. Middleton, W.D., and Carlson, H.W., "A Numerical Method for Calculating Near-Field Sonic-Boom Pressure Signatures", NASA TN D-3082, 1965.

17. Ritzel, D.V., "Numerical Evaluation of Whitham's F-Function for Supersonic Projectiles", AIAA Journal, 26 (2), 244-247, February 1988.

References (Continued)

18. Cotton, D., and Donn, W.L., "Sounds From Apollo Rockets in Space", Science, 171 (12), 565-567, 1971.

19. Garcia, F., Jr., Jones, J.H., and Henderson, H.R., "A Comparison of Measured and Theoretical Predictions for STS Ascent and Entry Sonic Booms", Shuttle Performance: Lessons Learned, Part 2, Arrington, J.P., and Jones, J.J., compilers, NASA CP 2283, Pt. 2, 1277-1301, 1983.

20. Blokhintzev, D.I., "The Propagation of Sound in an Inhomogeneous and Moving Medium I", J.Acoust.Soc.Am., 18, 322-328; also, "Acoustics of a Nonhomogeneous Moving Medium", Gostekhiazat, Moscow, USSR, 1946: translated as NACA TM-1399, 1946.

21. Officer, C.B., Introduction to the Theory of Sound Transmission, With Application to the Ocean, McGraw-Hill, New York, 1958.

22. Keller, J.B., "Geometrical Acoustics. I. The Theory of Weak Shock Waves", J.App.Mech., 25 (8), 938-947, 1955.

23. Thomas, C.L., "Extrapolation of Sonic Boom Pressure Signatures by the Waveform Parameter Method", NASA TN D-6832, June 1972.

24. Taylor, A.D., "The TRAPS Sonic Boom Program", NOAA Technical Memorandum ERL-87, July 1980.

25. Gardner, J.H., and Rogers, P.H., "Thermospheric Propagation of Sonic Booms From the Concorde Supersonic Transport", NRL Memorandum Report 3904, 1979.

26. George, A.R., and Kim, Y.N., "High-Altitude Long-Range Sonic Boom Propagation", J.Aircraft, 16, 637-639, 1979.

27. Rickley, E.J., and Pierce, A.D., "Detection and Assessment of Secondary Sonic Booms in New England", DOT-TSC-FA953-PR-79-2, 1978.

28. George, A.R., and Plotkin, K.J., "Sonic Boom Amplitudes and Waveforms in a Real Atmosphere", AIAA Journal, 7, 1978-1981, October 1969.

29. McLean, F.E., "Some Nonasymptotic Effects on the Sonic Boom of Large Airplanes", NASA TN D-2877, June 1965.

30. Carlson, H.W., "Simplified Sonic Boom Prediction", NASA Technical Paper 1122, 1978.

31. Hubbard, H.H., Maglieri, D.J., Huckel, V., and Hilton, D.A. (with appendix by Carlson, H.W.), "Ground Measurements of Sonic Boom Pressures for the Altitude Range of 10,000 to 75,000 Feet", NASA TR R-198, 1964.

32. Maglieri, D.J., Parrott, T.L., Hilton, D.A., and Copeland, W.L., "Lateral-Spread Sonic-Boom Ground-Pressure Measurements From Airplanes at High Altitudes to 75,000 Feet and at Mach Numbers to 2.0", NASA TN D-2021, November 1963.

33. Maglieri, D.J., "Sonic Boom Ground Pressure Measurements for Flights at Altitudes in Excess of 70,000 Feet and at Mach Numbers Up to 3.0", Second Conference on Sonic Boom Research, Schwartz, I.R. (Ed.), NASA SP-180, 1968.

References (Continued)

34. Green, K.S., and Putnam, T.W., "Measurements of Sonic Booms Generated by an Airplane Flying at Mach 3.5 and 4.8", NASA TM X-3126, October 1974.

35. Carlson, H.W., "An Investigation of Some Aspects of the Sonic Boom by Means of Wind-Tunnel Measurements of Pressures About Several Bodies at a Mach Number of 2.01", NASA TN D-161, 1959.

36. Carlson, H.W., "An Investigation of the Influence of Lift on Sonic-Boom Intensity by Means of Wind-Tunnel Measurements of the Pressure Fields of Several Wing-Body Combinations at a Mach Number of 2.01", NASA TN D-881, 1961.

37. Carlson, H.W., "Wind-Tunnel Measurements of the Sonic-Boom Characteristics of a Supersonic Bomber Model and a Correlation With Flight-Test Ground Measurements", NASA TM X-700, 1962.

38. Morris, O.A., "A Wind-Tunnel Investigation at a Mach Number of 2.01 of the Sonic-Boom Characteristics of Three Wing-Body Combinations Differing in Wing Longitudinal Location", NASA TN D-1384, 1962.

39. Carlson, H.W., "Correlation of Sonic Boom Theory With Wind Tunnel and Flight Measurements", NASA TR R-213, 1964.

40. Morris, O.A., Lamb, M., and Carlson, H.W., "Sonic-Boom Characteristics in the Extreme Near Field of a Complex Airplane Model at Mach Numbers of 1.5, 1.8, and 2.5", NASA TN D-5755, April 1970.

41. Hunton, L.W., "Current Research in Sonic Boom", Second Conference on Sonic Boom Research, Schwartz, I.R. (Ed.), NASA SP-180, 1968.

42. Hicks, R.M., Mendoza, J.P., and Thomas, C.L., "Pressure Signatures for the Apollo Command Module and the Saturn V Launch Vehicle With a Discussion of Strong Shock Extrapolation Procedures", NASA TM X-62, 117, April 1972.

43. Ashby, G.C., "Near-Field Sonic-Boom Pressure Signatures for the Space Shuttle Launch and Orbiter Vehicles at Mach 6", NASA TP-1405, April 1979.

44. Stansbery, E.G., and Stanley, J.F., "Sonic Boom Levels Measured for STS-41B Landing", LEMSCO-20864, September 1984.

45. Ashby, G.C., "A Study of the Sonic-Boom Characteristics of a Blunt Body at a Mach Number of 6", NASA TP 1787, December 1980.

46. Seebass, A.R., "Hypersonic Boom", Boeing Scientific Research Laboratories Technical Communication 030, June 1970.

47. Tiegerman, B., "Sonic Booms of Drag-Dominated Hypersonic Vehicles", Ph.D. Thesis, Cornell University, August 1975.

48. Seebass, A.R., and George, A.R., "Design and Operation of Aircraft to Minimize Their Sonic Boom", J.Aircraft, 11 (9), 509-517, September 1974.

49. Jones, L.B., "Lower Bounds for Sonic Bangs", J.Roy.Aeron.Soc., 65, 1-4, 1961. An *ad hoc* analysis of the same problem was given by Carlson, H.W., "The Lower Bound of Attainable Sonic-Boom Overpressure and Design Methods of Approaching This Limit", NASA TN D-1494, October 1962.

References (Continued)

50. Ferri, A., Ting, L., and Lo, R.W., "Nonlinear Sonic-Boom Propagation Including the Asymmetric Effects", AIAA Journal, 15 (5), 653-658, 1977.

51. Darden, C.M., "An Analysis of Shock Coalescence Including Three-Dimensional Effects With Application to Sonic Boom Extrapolation", NASA Technical Paper 2214, 1984.

52. Parker, L.W., and Zalosh, R.G., "Gudunov-Method Computation of the Flow Field Associated With a Sonic Boom Focus", AIAA Paper 73-240, 1973.

53. Sturtevant, B., and Kulkarny, V.A., "Dynamics of Weak Shock Waves at a Focus", in Noise and Vibration Control Engineering, Crocker, M.T. (Ed.), Purdue University Press, 402-415, 1971.

54. Wanner, J-C.L., Vallee, J., Vivier, C., and Thery, C., "Theoretical and Experimental Studies of the Focus of Sonic Booms", J.Acoust.Soc.Am., 52, 1972.

55. Onyeonwu, R.O., "Sonic Boom Signatures and Ray Focusing in General Maneuvers: I. Analytical Foundations and Computer Formulation; II: A Numerical Study", J.Sound Vib., 42 (1), 85-102; 103-114, 1975.

56. Plotkin, K.J., and Cantril, J.M., "Prediction of Sonic Boom at a Focus", Wyle Research Report WR 75-7, October 1975. Also, AIAA Paper 76-2, January 1976.

57. Plotkin, K.J., "Sonic Boom Focus Conditions Due to Tactical Air Operations", Wyle Research Report WR 84-8, February 1984.

58. Ludwig, D., "Uniform Asymptotic Expansions at a Caustic", Comm. on Pure and Appl Math, XIX, 215-250, 1966.

59. Guiraud, J.P., "Acoustique Geometrique, Bruit Ballistique des Avions Supersonique et Focalisation", J.Mecanique, 4, 215-267, 1965.

60. Gill, P.M., and Seebass, A.R., "Non-Linear Acoustic Behavior at a Caustic: An Approximate Solution",

61. Gill, P.M., "Nonlinear Acoustic Behavior at a Caustic", Ph.D. Thesis, Cornell University, June 1974.

62. Haglund, G.T., and Kane, E.J., "Analysis of Sonic Boom Measurements Near Shock Wave Extremities for Flight Near Mach 1.0 and for Airplane Accelerations", NASA CR-2417, 1974.

63. Sanai, J., Toong, T.-Y., and Pierce, A.D., "Ballistic Range Experiments on Super-booms Generated by Refraction", and "Ballistic Range Experiments on the Super-boom Generated at Increasing Flight Mach Numbers", J.Acoust.Soc.Am., 59 (3), 513-524, 1976.

64. Hayes, W.D., "Comments on the Caustic Problem", in Third Conference on Sonic Boom Research, Schwartz, I.R. (Ed.), NASA SP-255, October 1970.

65. Fung, K.Y., "Shock Wave Formation at a Caustic", SIAM J.Appl.Math, 39 (2), 355-371, October 1980.

66. Fung, K.Y., and Seebass, A.R., "Acoustic Behavior of a Discontinuous Signal Near a Caustic", Appendix B of NASA CR-2417, July 1974.

References (Continued)

67. Cramer, M.S., and Seebass, A.R., "Focus of Weak Shock Waves at an Arete", J.Fluid Mechanics, 88, 209-222, 1978.

68. Cramer, M.S., "Focusing of a Weak Three-Dimensional Shock Wave", AIAA Journal, 19 (10), 1363-1365, 1981.

69. Hilton, D.A., Huckel, V., and Maglieri, D.J., "Sonic Boom Measurements During Bomber Training Operations in the Chicago Area", NASA TN D-3655, 1966.

70. George, A.R., "The Effects of Atmospheric Inhomogeneities on Sonic Boom", in Third Conference on Sonic Boom Research, Schwartz, I.R. (Ed.), NASA SP-255, October 1970.

71. Pierce, A.D., and Maglieri, D.J., "Effects of Atmospheric Irregularities on Sonic-Boom Propagation", JASA, 51 (2), 702-721, 1972.

72. Chernov, L.A., Wave Propagation in a Random Medium, McGraw-Hill Book Col, 1960. Also, Dover, 1967.

73. Tatarski, V.I., Wave Propagation in a Turbulent Medium, McGraw-Hill Book Co., 1961. Also, Dover, 1967.

74. Keller, J.B., "Wave Propagation in Random Media", Proceedings of Symposia in Appl. Math., XIII, Hydrodynamic Instability, Amer. Math. Soc., Providence, 227-246, 1962.

75. Crow, S.C., "Distortion of Sonic Bangs by Atmospheric Turbulence", J.Fluid Mech., 37, 529-563, 1969; also, NPL Aero Report 1260.

76. Plotkin, K.J., and George, A.R., "Weak Shock Waves in Turbulent Media", AIAA Paper 70-54, January 1970.

77. Plotkin, K.J., "Perturbations Behind Thickened Shock Waves", in Third Conference on Sonic Boom Research, Schwartz, I.R. (Ed.), NASA SP-255, October 1970.

78. Plotkin, K.J., and George, A.R., "Propagation of Weak Shock Waves Through Turbulence", J.Fluid Mechanics, 54 (3), 449-467, 1972.

79. Plotkin, K.J., "The Effect of Atmospheric Inhomogeneities on the Sonic Boom", Ph.D. Thesis, Cornell University, 1971.

80. Pierce, A.D., "Statistical Theory of Atmospheric Turbulence on Sonic Boom Rise Times", J.Acoust.Soc.Am., 49, 906-924, 1971.

81. Ffowcs-Williams, J.E., and Howe, M.S., "On the Possibility of Turbulent Thickening of Weak Shock Waves", J.Fluid Mech., 58, 461-480, 1973.

82. Tubb, P.E., "Measured Effects of Turbulence on the Rise Time of a Weak Shock", AIAA Paper 75-543, March 1975.

83. Bass, H.E., Layton, B.A., and Bolen, L.N., "Propagation of Medium Strength Shock Waves Through the Atmosphere", J.Acoust.Soc.Am., 82 (1), 306-310, July 1987.

84. American National Standards Institute, "American National Standard Method for the Calculation of the Absorption of Sound by the Atmosphere", ANSI S1.26-1978 (ASA 23-1978).

References (Continued)

85. Bass, H.E., Ezell, J., and Raspet, R., "Effect of Vibrational Relaxation on Rise Times of Shock Waves in the Atmosphere", JASA, 74 (5), 1514-1517, 1983.

86. Ferri, A., "Airplane Configurations for Low Sonic Boom", Third Conference on Sonic Boom Research, SP-255, 255-275, 1971.

87. Darden, C.M., "Sonic Boom Minimization With Noise Bluntness Relaxation", NASA TP 1348, 1979.

88. Mack, R.J., and Darden, C.M., "Some Effects of Applying Sonic Boom Minimization to Supersonic Cruise Aircraft Design", J.Aircraft, 17 (3), 182-186, March 1980.

89. Plotkin, K.J., "Focus Boom Footprints for Various Air Force Supersonic Operations", Wyle Research Report WR 85-22, 1985.

90. Galloway, W.J., "Development of C-Weighted Day-Night Average Sound Level Contours for F-15 Air Combat Maneuvering Areas", BBN Report 4430, August 1980.

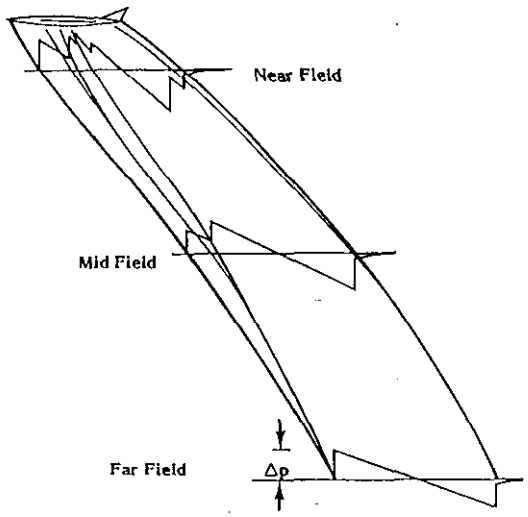

Figure 1. Sonic Boom Generation, Propagation, and Signature Evolution.

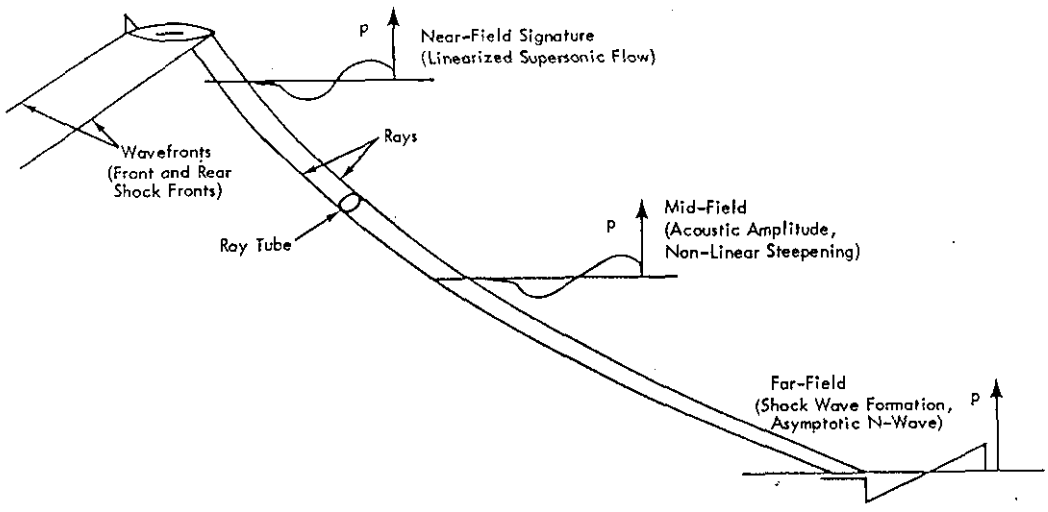

Figure 2. Sonic Boom Generation and Propagation: Ray Viewpoint.

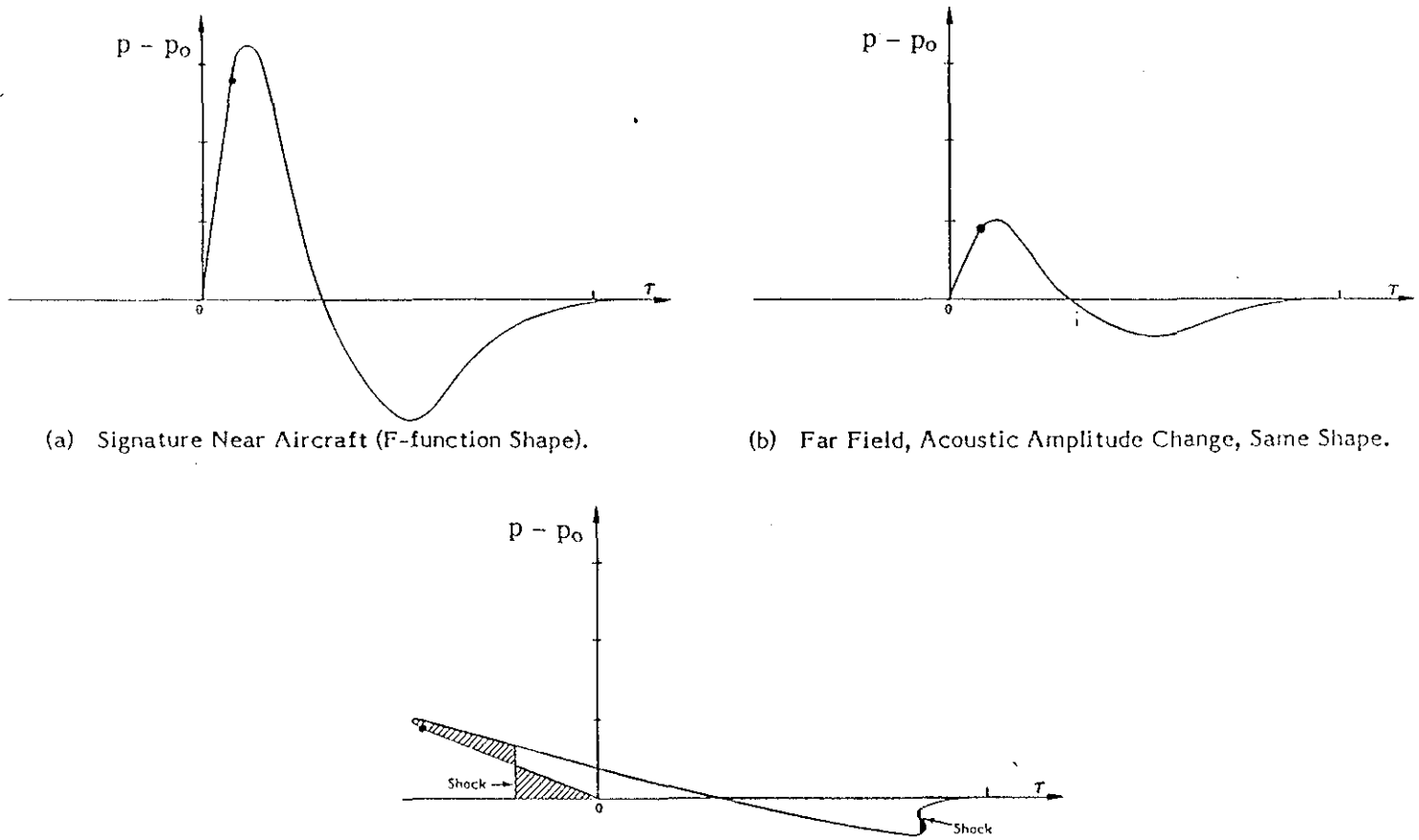

(a) Signature Near Aircraft (F-function Shape).

(b) Far Field, Acoustic Amplitude Change, Same Shape.

(c) Far-Field Steepened (Aged) Signature.

Figure 3. Evolution and Steepening of Sonic Boom Signatures.

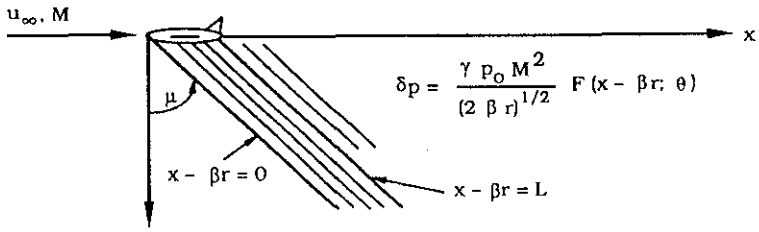

Figure 4. Linearized Flow (Area Rule) Theory.

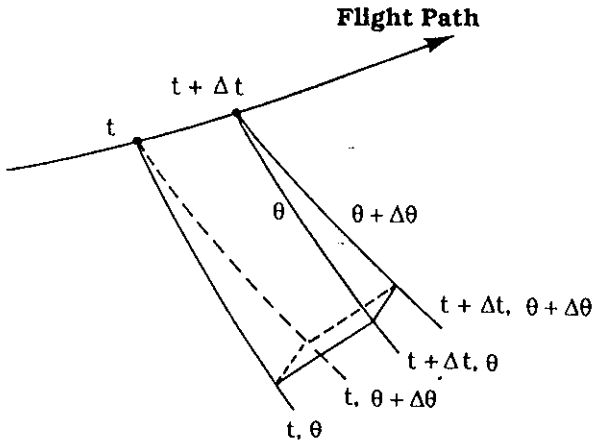

Figure 5. Ray Tube Outlined by Four Corner Rays Δt and Δθ Apart.

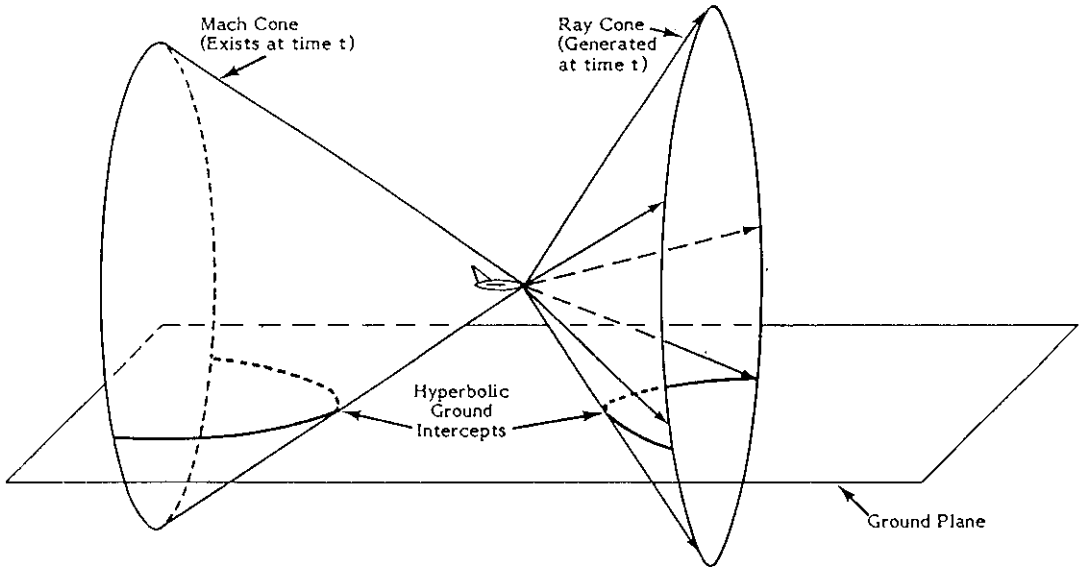

Figure 6. Mach and Ray Cones in Supersonic Flight.

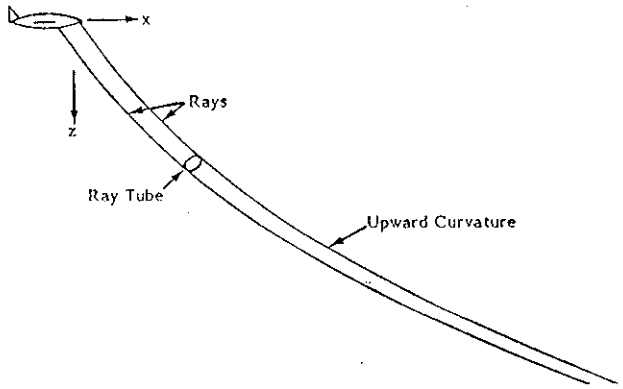

(a) Rays Under Flight Track.

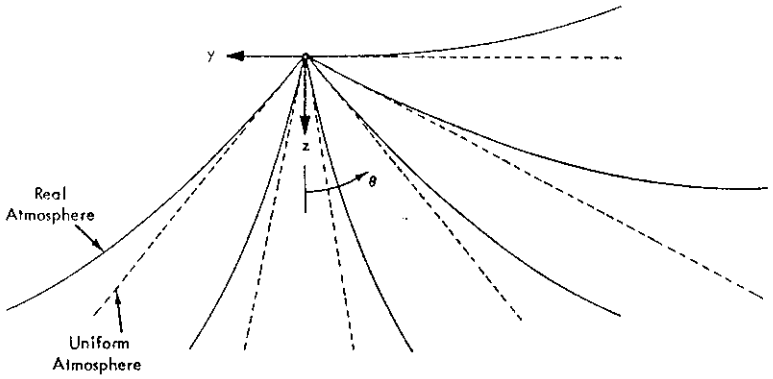

(b) Rays Across Flight Track.

Figure 7. Curvature of Sonic Boom Rays in the Atmosphere.

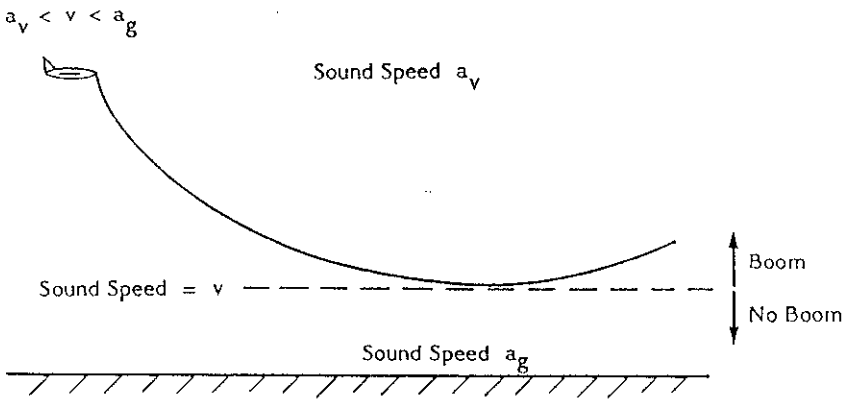

Figure 8. Flight at Sonic Cutoff Condition.

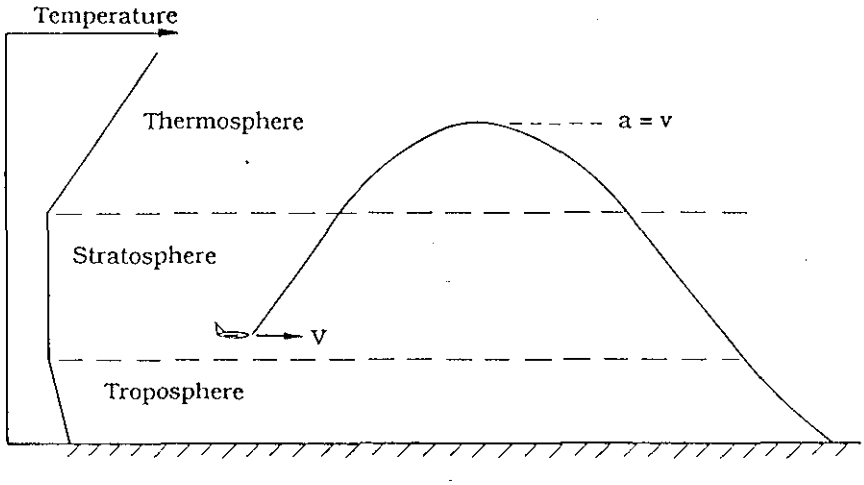

Figure 9. Over-the-Top Sonic Boom Ray Path.

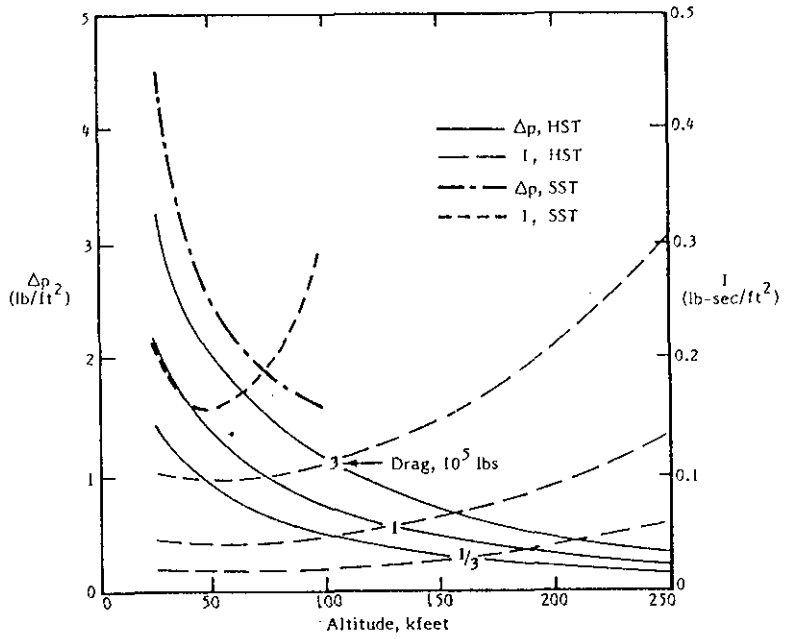

Figure 10. Overpressure and Impulse as a Function of Altitude for Drag-Dominated Hypersonic Vehicle. Conventional SST shown for comparison.

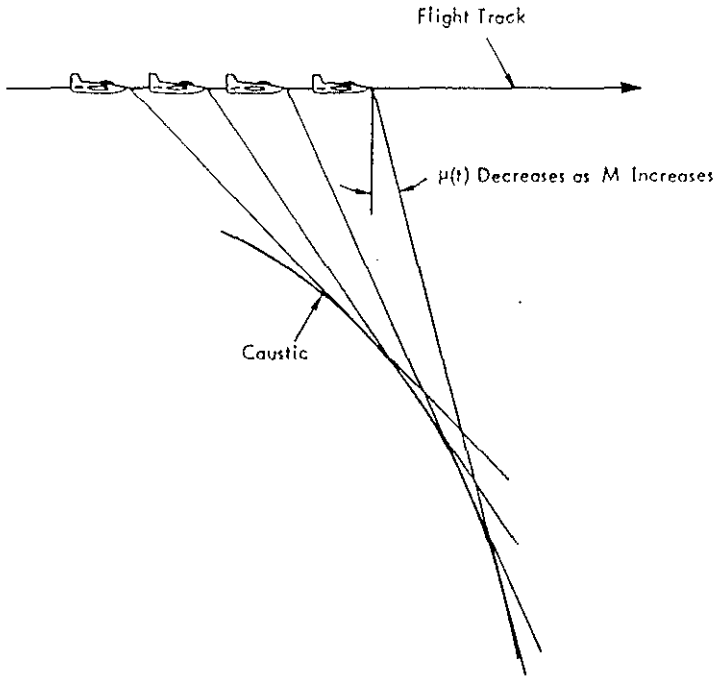

Figure 11. Sonic Boom Focus Due to Acceleration.

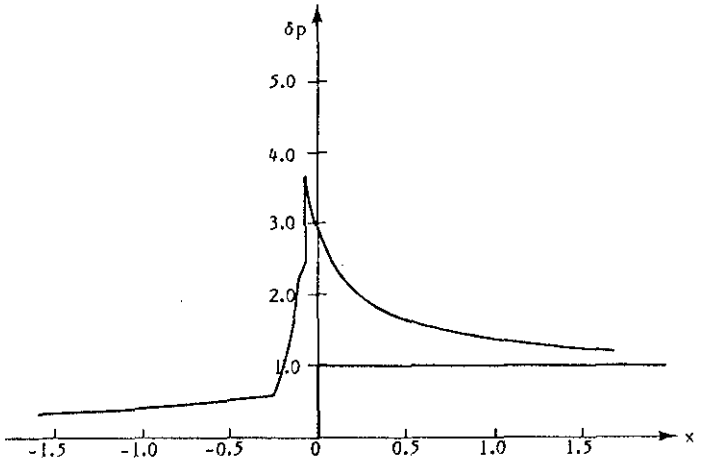

Figure 12. Gill-Seebass Solution for Focused Shock Wave.

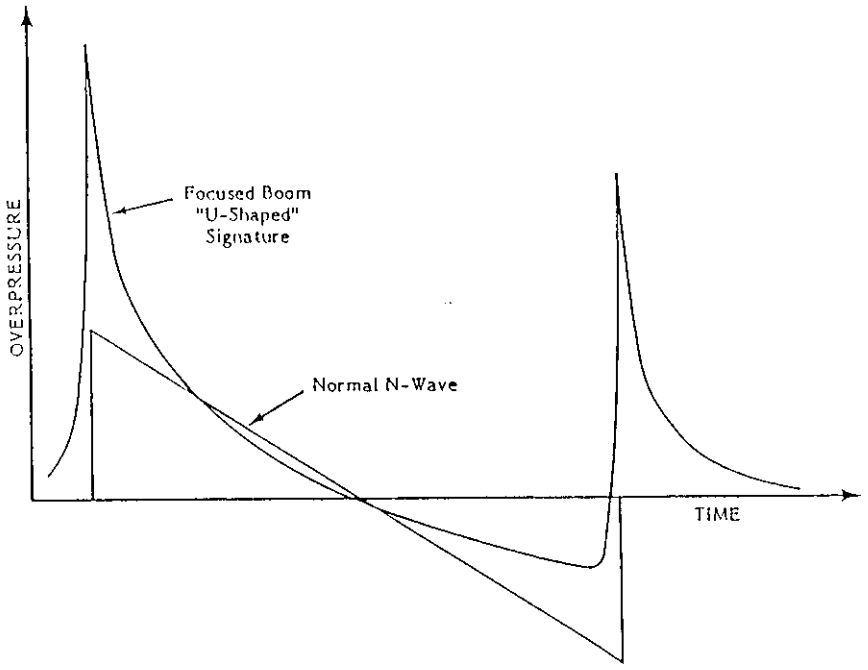

Figure 13. Focused and Unfocused Boom Signatures.

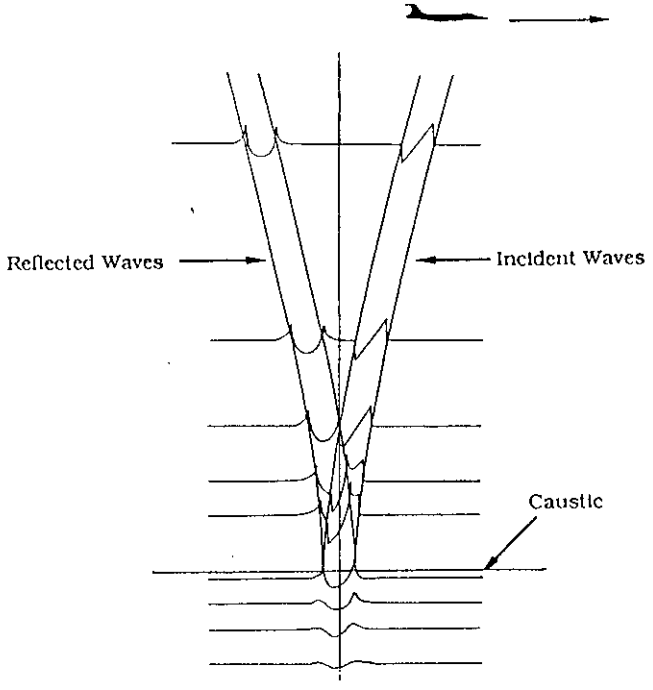

Figure 14. Typical Wave Patterns and Signatures Near a Caustic.[62]

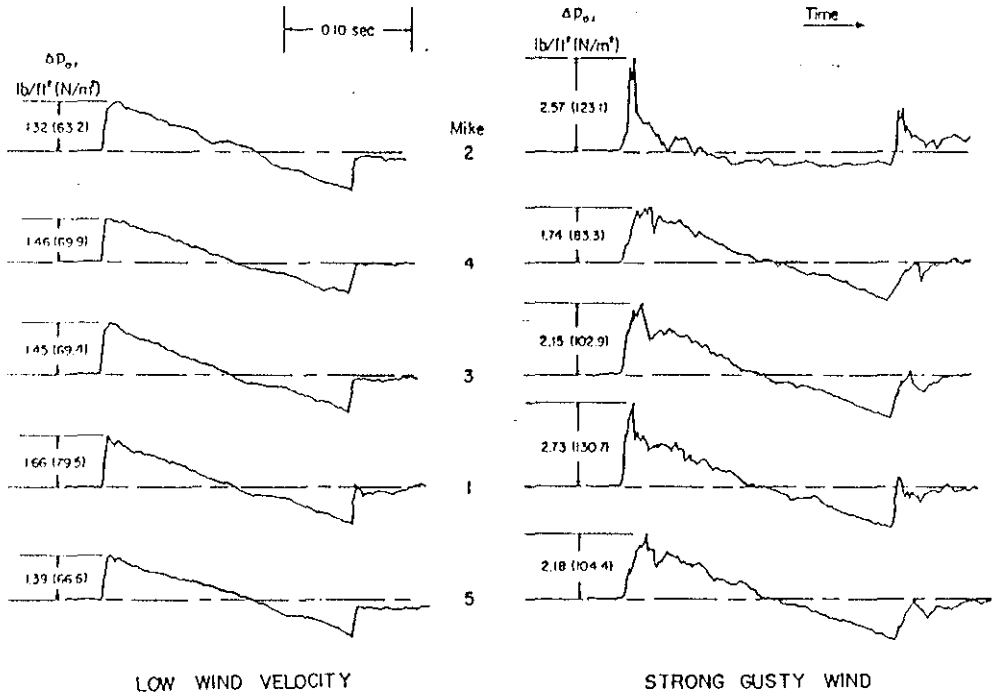

Figure 15. Sonic Boom From Two Flights Under Different Atmospheric Conditions.[68]

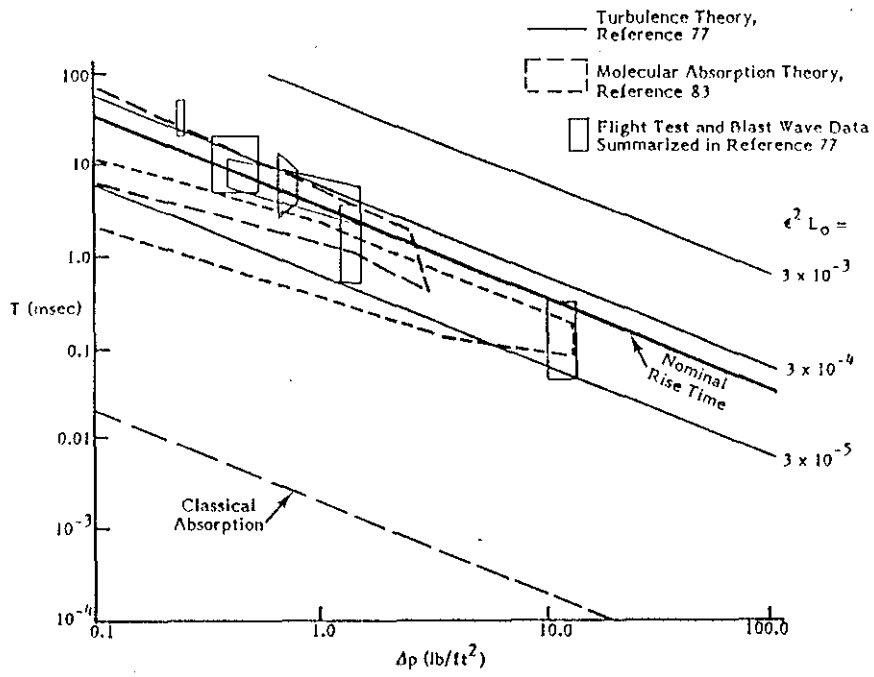

Figure 16. Shock Wave Rise Time Theories and Measurements.